

**BULETINUL
INSTITUTULUI
POLITEHNIC
DIN IAȘI**

Tomul LX (LXIV)

Fasc. 1-2

ȘTIINȚA ȘI INGINERIA MATERIALELOR

2014

Editura POLITEHNIUM

BULETINUL INSTITUTULUI POLITEHNIC DIN IAȘI
PUBLISHED BY
„GHEORGHE ASACHI” TECHNICAL UNIVERSITY OF IAȘI
Editorial Office: Bd. D. Mangeron 63, 700050, Iași, ROMANIA
Tel. 40-232-278683; Fax: 40-232 237666; e-mail: polytech@mail.tuiasi.ro

Editorial Board

President : Prof.dr.eng. **Ion Giurma**, Member of the Academy of Agricultural Sciences and Forest, *Rector* of the "Gheorghe Asachi" Technical University" of Iași

Editor-in -Chief : Prof.dr.eng. **Carmen Teodosiu**, *Vice-Rector* of the "Gheorghe Asachi" Technical University of Iași

Honorary Editors of the Bulletin: Prof.dr.eng. **Alfred Braier**

Prof.dr.eng. **Hugo Rosman**

Prof.dr.eng. **Mihail Voicu**, Corresponding Member of the Romanian Academy

Editors in Chief of the MATERIALS SCIENCE AND ENGINEERING Section

Assoc. Prof. Dr. Eng. **Iulian Ioniță**

Assoc. Prof. Dr. Eng. **Gheorghe Bădărău**

Prof. Dr. Eng. **Dan Gelu Gălușcă**

Prof. Dr. Eng. **Costică Bejinariu**

Honorary Editors: Prof. Dr. Eng. **Ion Hopulele**, Prof. Dr. Eng. **Ion Mălureanu**,

Prof. Dr. Eng. **Adrian Dima**

Associated Editor: Assoc. Prof.Dr. Eng. **Ioan Rusu**

Editorial Advisory Board

Prof.dr.eng. **Agustin Santana Lopez**, La Palmas de Gran Canaria University, (Spain)

Prof.dr.eng. **Mihai Susan**, Technical University "Gheorghe Asachi" from Iasi, (Romania)

Prof.dr.eng. **Ioan Carcea**, Technical University "Gheorghe Asachi" from Iasi, (Romania)

Prof.dr. **Duu-Jong Lee**, National Taiwan University of Science and Technology, (Taiwan)

Prof.dr.eng. **Shih-Hsuan Chiu**, National Taiwan University of Science and Technology, (Taiwan)

Prof.dr.eng. **Yuri A. Burennikov**, Vinnitsya National Technical University, (Ukraine)

Prof. dr. **Oronzio Manca**, Seconda Università degli Studi di Napoli (Italy)

Prof.dr.eng. **Julia Mirza Rosca**, La Palmas de Gran Canaria University, (Spain)

Prof.dr.eng. **Petrică Vizureanu**, Technical University "Gheorghe Asachi" from Iasi, (Romania)

Assoc. Prof. **Shizutoshi Ando**, Tokyo University of Sciences, (Japan)

Prof.dr.eng. **Leandru-Gheorghe Bujoreanu**, Technical University "Gheorghe Asachi" from Iasi, (Romania)

Prof. dr. eng. **Constantin Baciu**, Technical University "Gheorghe Asachi" from Iasi, (Romania)

Dr. **Koichi Tsuchiya**, National Institute for Materials Science (Japan)

Dr.eng. **Burak Özkal**, Istanbul Technical University (Turkey)

Prof. dr. eng. **Vasile Cojocaru-Filipiuc**, Technical University "Gheorghe Asachi" from Iasi, (Romania)

Prof. dr. **Viorel Păun**, University "Politehnica" Bucharest, (Romania)

Prof.dr. **Maricel Agop**, Technical University "Gheorghe Asachi" from Iasi, (Romania)

Prof.dr.eng. **Sergiu Stanciu**, Technical University "Gheorghe Asachi" from Iasi, (Romania)

ȘTIINȚA ȘI INGINERIA MATERIALELOR

S U M A R

	<u>Pag.</u>
OANA BĂLȚĂTESCU, RALUCA-MARIA FLOREA, IOAN RUSU și IOAN CARCEA, Analiza SEM a spumelor metalice pe bază de AlMg cu adaos de SiC (engl. rez. rom.)	9
GHEORGHE BULUC, IULIA FLOREA și IOAN CARCEA, Aliaje cu entropie ridicată – o nouă lume a materialelor (engl. rez. rom.)	23
MANUELA-CRISTINA PERJU, CARMEN NEJNERU, MIHAI AXINTE și CĂTĂLIN-ANDREI ȚUGUI, Studii asupra aderenței straturilor cu depunere prin descărcare electrică în impuls pe suport de oțel slab aliat (engl. rez. rom.)	29
VASILE COJOCARU-FILIPUIC, Albirea fontei în cazul elaborării fontei cenușii în cantitate mică (engl. rez. rom.)	37
VASILE COJOCARU-FILIPUIC, Metodă de producere a fontei cu grafit compactizat (engl. rez. rom.)	45
VASILE COJOCARU-FILIPUIC și DANIELA-LUCIA CHICET, Mecanismul obținerii grafitului nodular, prin modificare, pentru o fontă tehnică, cu modificador lichid la temperatura de modificare (engl. rez. rom.)	53
FLORIN SĂNDULACHE, SERGIU STANCIU, NICANOR CIMPOEȘU și RAMONA CIMPOEȘU, Aplicații ale materialelor metalice biodegradabile (engl. rez. rom.)	63
MARIA-LUCIANA ATOMEI, Inovarea în societatea bazată pe cunoaștere. Tehnologia de sudare a plasticelor (engl. rez. rom.)	75
ANIȘOARA CORĂBIERU, PETRICĂ CORĂBIERU și DAN-DRAGOȘ VASILESCU, Procedeu combinat de obținere a pieselor multistrat (engl. rez. rom.)	87

MATERIALS SCIENCE AND ENGINEERING

CONTENTS

	<u>Pp.</u>
OANA BĂLȚĂTESCU, RALUCA-MARIA FLOREA, IOAN RUSU and IOAN CARCEA, SEM Analysis of AlMg Foams with SiC Addition (English, Romanian summary)	9
GHEORGHE BULUC, IULIA FLOREA and IOAN CARCEA, High Entropy Alloys – A New World a Materials (English, Romanian summary)	23
MANUELA-CRISTINA PERJU, CARMEN NEJNERU, MIHAI AXINTE and CĂTĂLIN-ANDREI ȚUGUI, Studies Regarding the Adherence of the Electro-Spark Deposition Coating Layer on the Heat Treated Low Alloy Steel Support (English, Romanian summary)	29
VASILE COJOCARU-FILIPCIUC, Iron Whitening when Manufacturing Grey Cast Iron in Small Amount (English, Romanian summary)	37
VASILE COJOCARU-FILIPCIUC, Method for Production of Compacted Graphite Cast Iron (English, Romanian summary)	45
VASILE COJOCARU-FILIPCIUC and DANIELA-LUCIA CHICET, Nodular Graphite Obtaining Mechanism, by Modification, for a Technical Iron, by a Liquid Inoculating Agent at the Inoculating Temperature (English, Romanian summary)	53
FLORIN SĂNDULACHE, SERGIU STANCIU, NICANOR CIMPOEȘU and RAMONA CIMPOEȘU, Biodegradable Metallic Materials Applications (English, Romanian summary)	63
MARIA-LUCIANA ATOMEI, Innovation in Knowledge Based Society. Plastics Welding Technology (English, Romanian summary)	75
ANIȘOARA CORĂBIERU, PETRICĂ CORĂBIERU and DAN-DRAGOȘ VASILESCU, Combined Process for Obtaining the Parts Multilayer (English, Romanian summary)	87

BULETINUL INSTITUTULUI POLITEHNIC DIN IAȘI
Publicat de
Universitatea Tehnică „Gheorghe Asachi” din Iași
Tomul LX (LXIV), Fasc. 1-2, 2014
Secția
ȘTIINȚA ȘI INGINERIA MATERIALELOR

SEM ANALYSIS OF AlMg FOAMS WITH SiC ADDITION

BY

OANA BĂLȚĂTESCU*, **RALUCA-MARIA FLOREA**, **IOAN RUSU**
and IOAN CARCEA

“Gheorghe Asachi” Technical University of Iași
Faculty of Material Science and Engineering

Received: January 10, 2014

Accepted for publication: January 27, 2014

Abstract: The paper presents several results related to the research of the AlMg10 metallic alloy based metallic foams, obtained by adding SiC particles in the melting, while bubbled with C₄H₁₀. The micro-structure of this foam is analyzed by using SEM, highlighting the intermingling pore networks developed around the SiC particles, as well as other characteristic micro-structural aspects. The foam formed on the melting surface has been removed using a specially designed device, adapted to the respective oven. After cooling in the air, samples specially adapted for the scanning electron microscope study have been taken from the obtained foam.

Keywords: metal foam; Al-Mg alloy; cellular composite.

1. General Considerations

Aluminum foams are a new class of materials with low densities, large specific surface and novel physical and mechanical properties. Their applications are extremely varied: for light weight structural components, for filters and electrodes and for shock or sound absorbing products. Recently, interesting foaming technology developments have proposed metallic foams as

*Corresponding author: *e-mail*: oana84rou@yahoo.com

a valid commercial chance; foam manufacturing techniques include solid, liquid or vapor state methods. The foams presented in this study are produced by Melt Gas Injection (MGI) process starting from melt aluminum (Wood, 1997). The injected air causes' bubbles to rise to the surface of the melt, forming liquid foam which is stabilized by the presence of solid ceramic particles on the gas liquid interfaces of the cell walls. The stabilized liquid foam is then mechanically conveyed off the surface of the melt and allowed to cool to form a solid slab of aluminum foam (Babcsán *et al.*, 2005). The aluminum foam structure (cell size and cell wall thickness) is controlled by the process variables such as the volume fraction of the solid particles; foaming temperature, airflow rate, and impeller design the foam making process. Unfortunately, no publication has been found in the work on the influence of the process in variables on the cell structure of aluminum foam (Asholt, 1999).

2. Experimental Results

The experimental equipment consists of an electric resistance furnace (maximum heating temperature 800°C), which was adapted for insufflations gas (SO₂, N₂, inert gas, etc.) It is also equipped with a wide agitator and a trough acquisition of foam formed.

It has been obtained metal foam by mixing the alloy melt AlMg10 with 10% SiC powder 120 μm size, at a temperature of 710°C and with C₄H₁₀ injection at 1.2 atm pressure (Bălătescu *et al.*, 2014).

The foam formed on the melting surface has been removed using a specially designed device, adapted to the respective oven. After cooling in the air, samples specially adapted for the scanning electron microscope study have been taken from the obtained foam.

Below we present the characterization of morphology and dimensional tests of samples from cell-based composite type aluminum alloy reinforced with silicon carbide particles. Analysis was performed by scanning electron microscopy (SEM) and the electron diffraction analysis (EDX).

Fig. 1 presents the general aspect of the composite and the general morphology of its constituents, as well as the pore distribution in the composite matrix. As the figure shows, the pores are intermingled and there are porous ligaments bridges between them.

The analysis on the distribution and the morphology for the carbides and the porosity formed in the composite structure leads to the conclusion that the material contains a multitude of carbides and pores with dimensions of over 50 μm in its volume (Fig. 2).

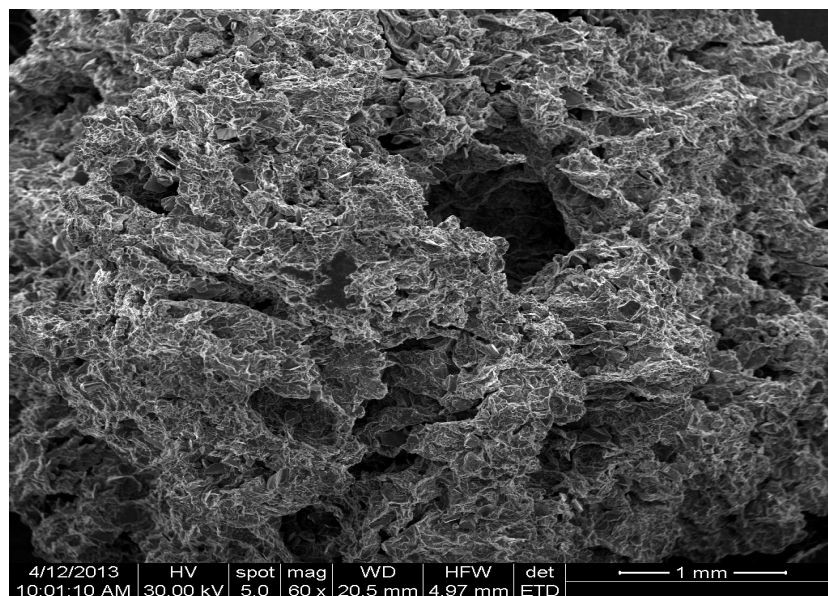


Fig. 1 – SEM electronic microscopy analysis highlighting the general aspect of the composite.

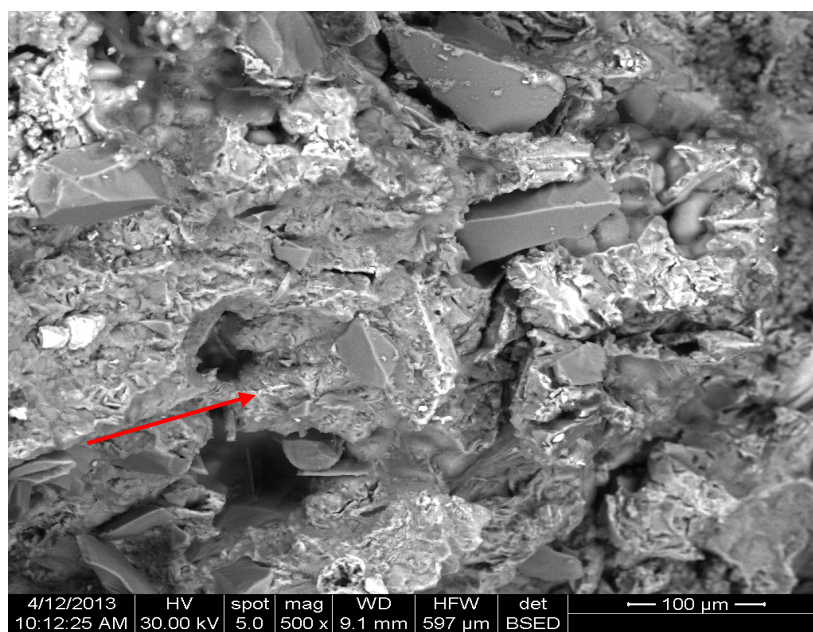


Fig. 2 – SEM image highlighting the distribution and the morphology for the carbides and the porosity formed in the composite structure.

The EDX analysis (Fig. 3) presents the distribution maps for the main composite constituents (Al, Si, Fe, Cu, Mg, O and C). The uniform distribution of these constituents may be observed, and also, the absence of the little spheres of aluminum oxide morphologic constituents from the composite matrix and the channels walls. The pore network developed around the silica carbides.

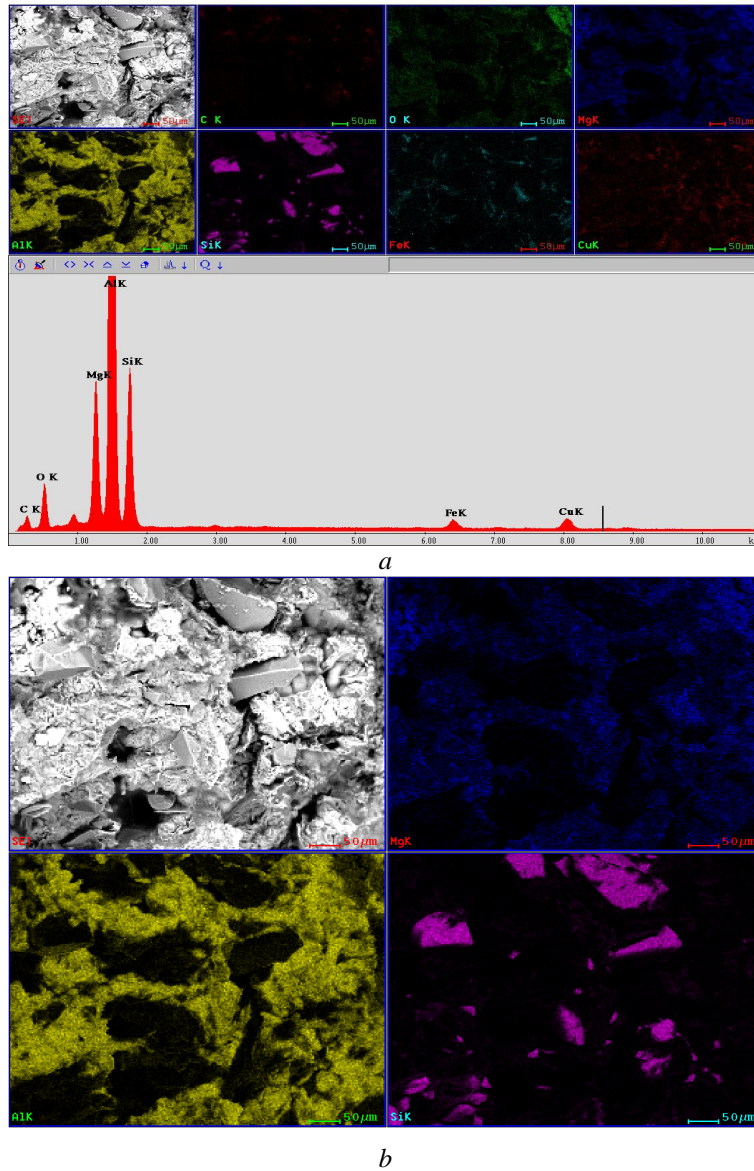


Fig. 3 – EDX electron diffraction analysis on the AlMg10 metallic foam sample (a) and the distribution maps for the main composite constituents – Al, Mg, Si (b)

Fig. 4 shows ligaments in different parts of the composite and the pore communication channels. The pointed zone shows the interior construction of the walls that create the porous area (A area). The flow of the gas through the liquid alloy, subsequently dendritic solidified, created pores with profiled walls that communicate among the whole composite body. The composite section highlights, in B area, the embedding of some very fine silica carbides in the matrix. The pores are missing in the adjacent areas (Fig. 5), compared to the areas including silica carbides with larger sizes (around 50...100 μm).

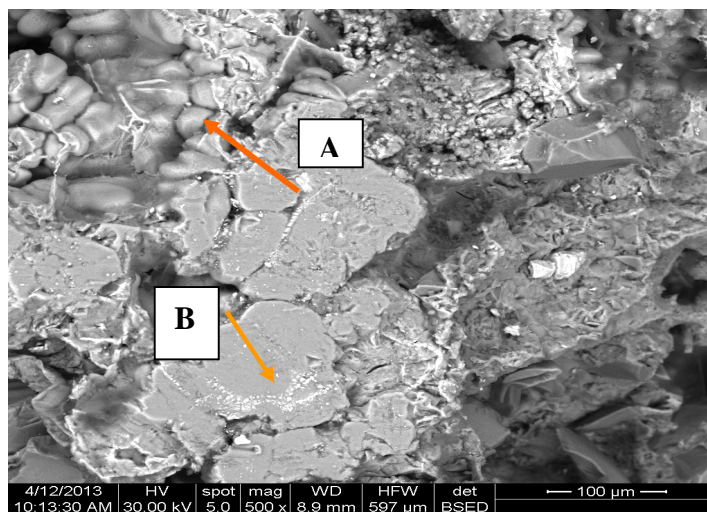


Fig. 4. SEM image with a section of the composite volume.

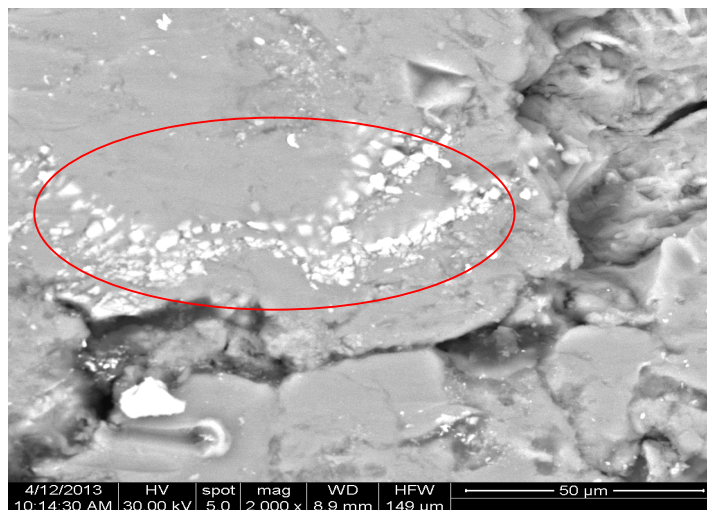


Fig. 5 – Detailed SEM image highlighting the area embedding very fine silica carbides.

The embedding way of the silica carbides in the inter-pore ligament walls and the pore intercommunication area can be observed in Fig. 6.

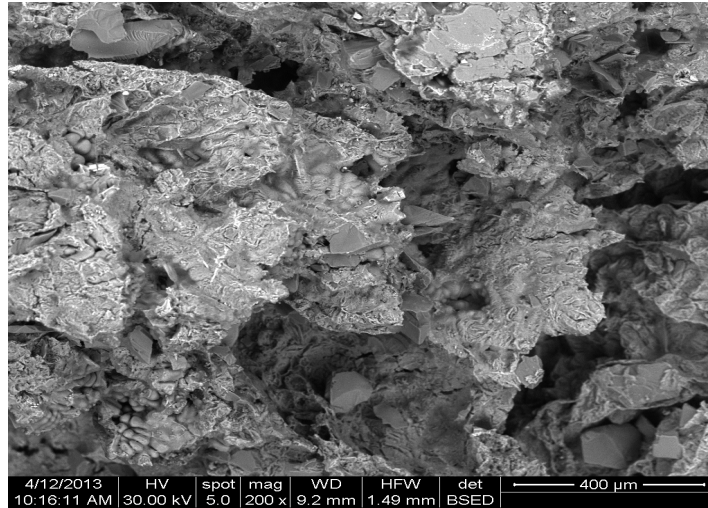


Fig. 6 – Detail for the embedding of the silica carbides in the inter-pore ligament walls.

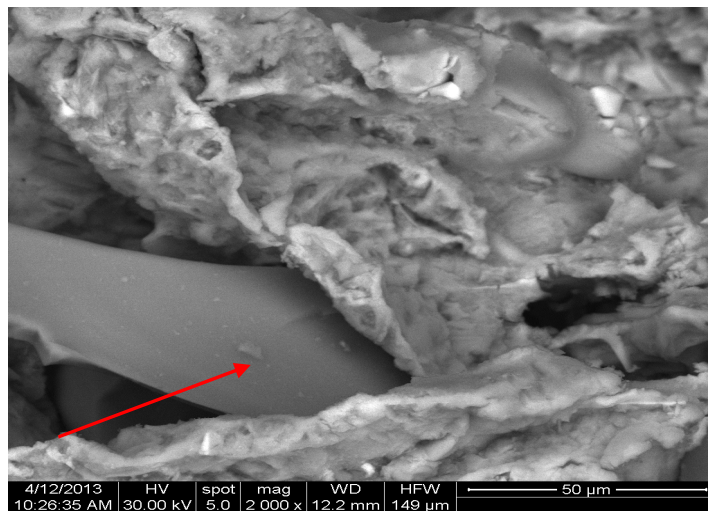


Fig. 7 – SEM image with the matrix solidification way around the silica carbides particles.

The SEM image with the matrix solidification way around the silica carbides particles (Fig. 7) shows that a strong separation of the alloy matrix appears in the interface area, with no adherence in the matrix-carbides contact area. It is possible that, when bubbling the butane, it flowed on the carbon particle surface, thus increasing the tendency to detach of the carbides from the matrix, substantially contributing to the composite porosity increase.

Fig. 8 presents the general morphology of the walls of interstices between the pores formed in the composite matrix, and Fig. 9 highlights the emplacement and the size for carbides and pore intercommunication bridges.

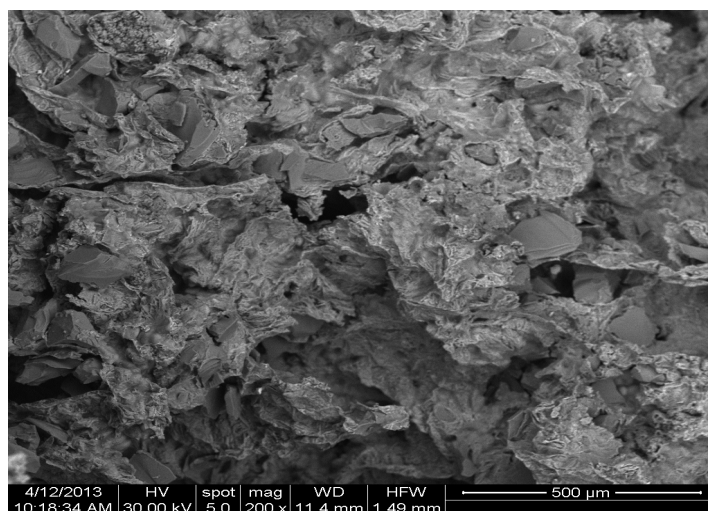


Fig. 8 – SEM image for the internal morphology of walls of interstices between the pores

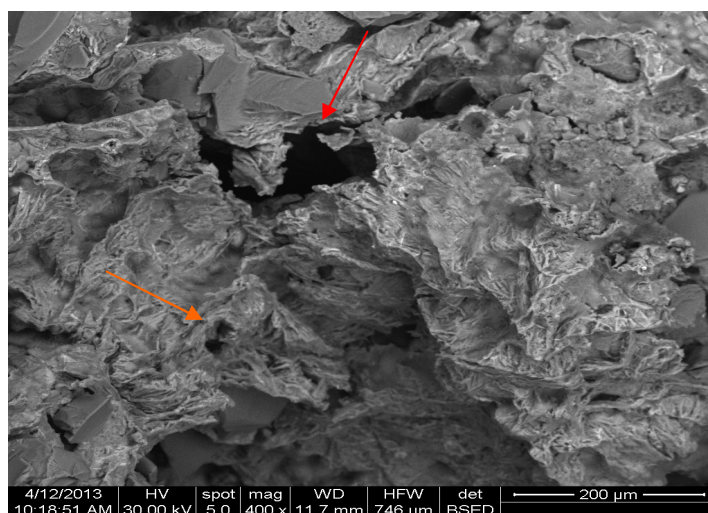


Fig. 10 – Detail image of the cavity surface morphology.

Figs. 10 and 11 present the morphology of the cavities found in the composite matrix. The “spongy” structure of the matrix and a multitude of multi-filamentous increases may be observed. These represent formations resulted by segregating the AlMgSi compounds, which appeared when the

matrix solidified, mostly on the solidification area of the formed cavities. Fig. 11 shows the spongy consistency of the cells, but also the existence of a micro-laminated or sharp aspect. We consider that it appeared as a result of the insertion of the modeling gas (butane), which was introduced in the whole mass of the composite before the solidification started.

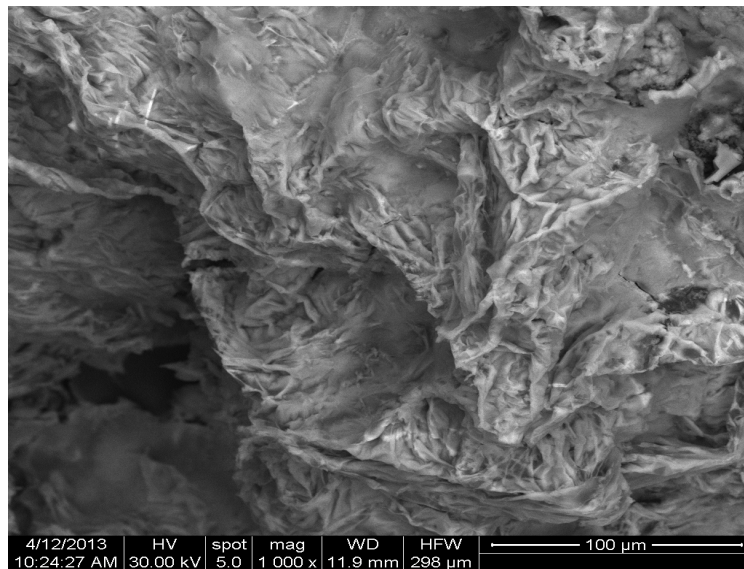


Fig. 11 – SEM analysis of the formed cells morphology.

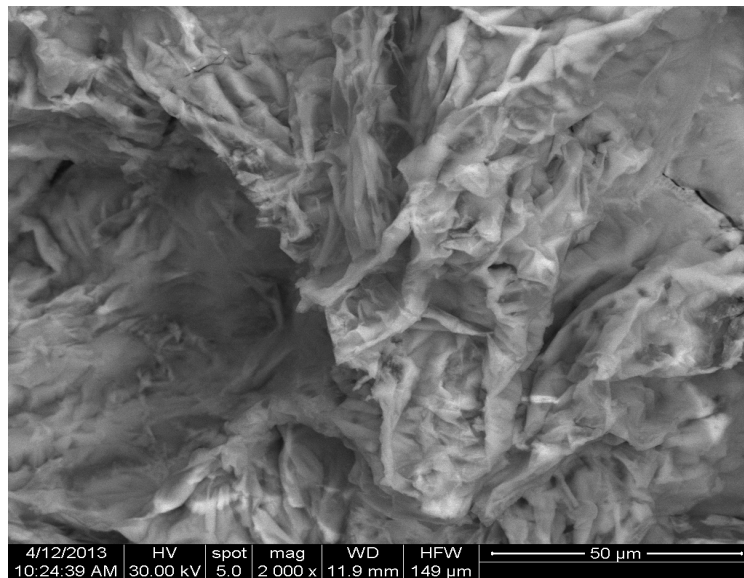


Fig. 12 – SEM micrograph highlighting the sharp aspect of the cells walls.

Figs. 12,...,14 present the sharp aspect of the cells walls forming the voids in the composite matrix. The resulted cavities are separated by connection bridges which have the same morphology and consistency as the cavities. A higher magnification power (Fig. 13) highlights the solidification way of the cells walls in a sharp type morphological structure; The “packaging” way of the sharp sheets forming the alloy spongy structure is easily observed. The sharp sheet solidification micro-structure of the cells walls found in the composite matrix (Fig. 14) depends of the flow direction for the gas which was dispersed in the melting, as well as of the advancing way of the solidification front in the composite matrix.

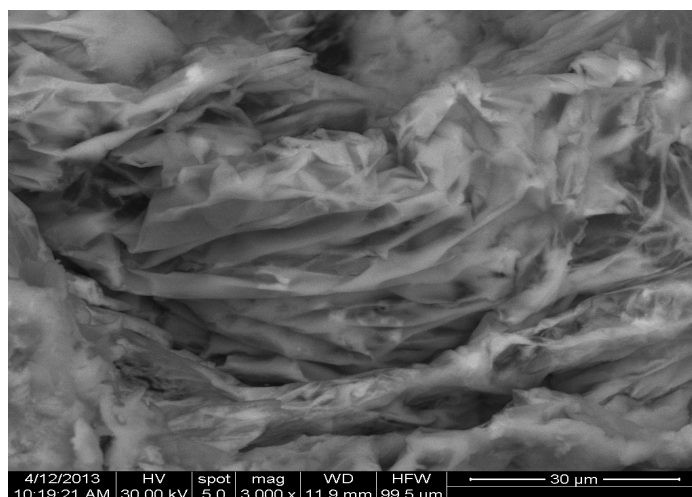


Fig. 13 – SEM detail highlighting the solidification way of the cells walls.

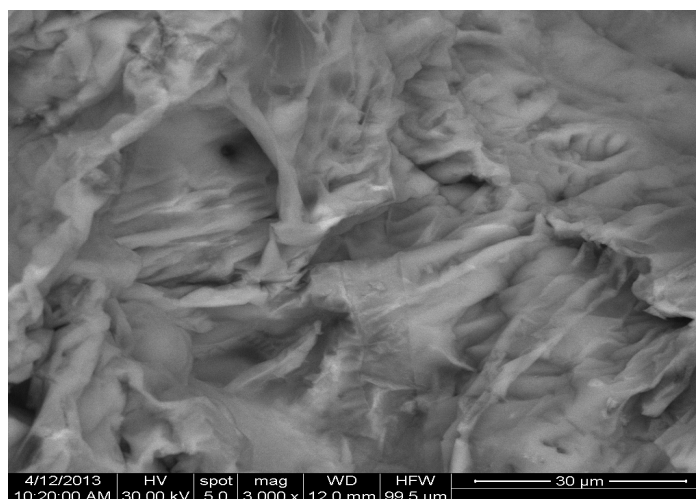


Fig. 14 – Cells walls solidification micro-structural morphologies.

Fig. 15 presents the development and solidification ways for a sharp aspect structure. The fact that between the different formed sharp sheets there are spaces ranging up to $10\ \mu\text{m}$ may be observed. The solidification sheets have a relative consistency and thickness ranging from 1 to $2\ \mu\text{m}$.



Fig. 15 – SEM detail of a sharp aspect structure.

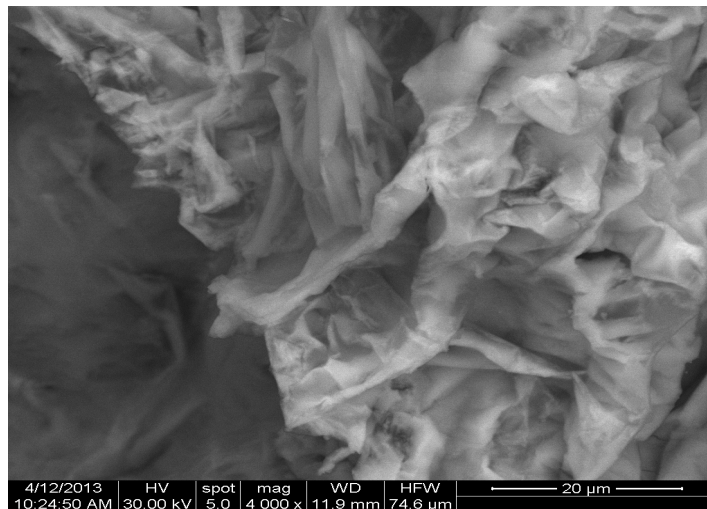


Fig. 16 – SEM image of the connection bridges created between the pores.

The connection bridges formed between the pores have a very low compactness structure, a fact proved by the multitude of porous volumes and communication channels between the solidified areas (Fig. 16). This aspect gives the composite an even greater degree of porosity.

The resulted contraction cracks that occurred at the matrix solidification and the complex silica crystallites (white-grey color in the image) that resulted at the alloy solidification can be observed in the cavities walls (Fig. 17).

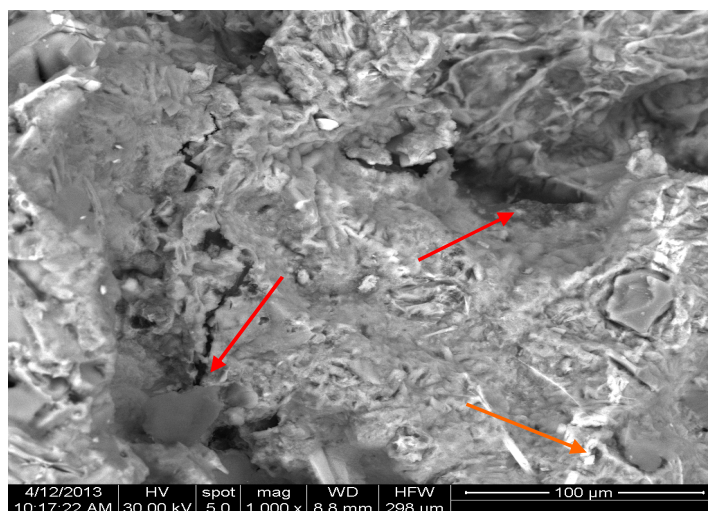


Fig. 17 – SEM image of the micro- cracks in the cavities walls.

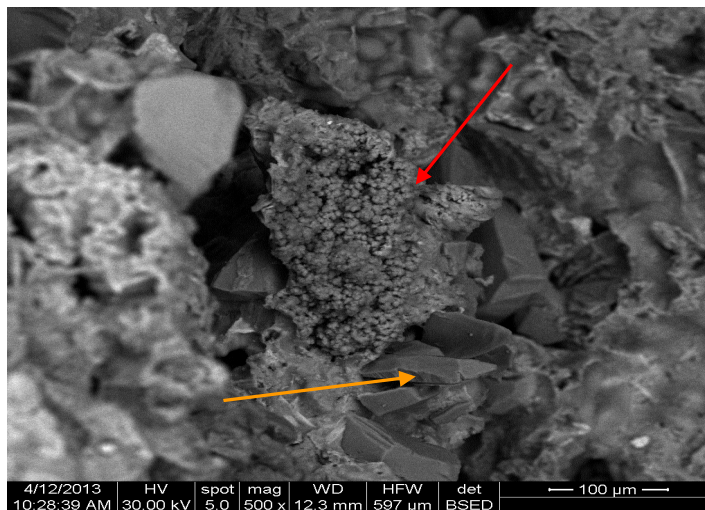


Fig. 18 – SEM image of the metallic foam microstructure highlighting the cluster structure.

In the foam microstructure it was observed the appearance of some cluster structure formations (Fig. 18), which are found in the carbides agglomeration areas. Thus, in the concentration areas and around the silica carbides agglomerations, as a result of inhomogeneous gas bubbling, sharp

conglomerates and also cluster structure conglomerates may be formed in the composite matrix. The advanced degree of porosity that exists in these solidification morphologies can be observed.

3. Conclusions

The SEM microstructure analysis lead to the following conclusions:

AlMg10 matrix type metallic foam obtained through C_4H_{10} bubbling with SiC addition presents intermingled pores, stabilized by the SiC particles, around which the pore network is developed.

In the areas adjacent to the very fine Si carbons agglomerations, the pores are missing, compared to the areas that include greater dimension silica carbides (around 50...100 μm).

There is no adherence in the matrix-carbides interface area, a phenomenon possibly determined by the entry of the blown gas in this area.

The AlMgSi compounds and the gas bubbles determine the formation of a spongy structure and a sharp aspect of the composite matrix cavities surface.

The inhomogeneous bubbling of gas used for the creating the metallic foam determines the appearance of sharp sheets and cluster structures conglomerates in the microstructure.

REFERENCES

- Asholt P., *Aluminium Foam Produced by the Melt Foaming Route Process, Properties and Applications*. Proc. of Int. Conf. on Metal Foam and Porous Metal Struct., MIT Publ., 133-140 (1999).
- Babcsán N., Garcia-Moreno F., Banhart J., *Role of Oxidation During Blowing of Aluminum Foams by External Gas Injection*. In: Nakajima, H., Kanetake, N. (Eds.), *Porous Metals and Metal Foaming Technol.*, Japan, 261–266, 2005.
- Bălătescu O., Nuțescu C., Rusu I., Roman C., Carcea I., *Microstructure Researches of Metallic Composite Foams Based on AlMg Alloys*. Adv. Materials Res., **1036**, 106-110 (2014).
- Banhart J., *Manufacture, Characterization and Application of Cellular Metals and Metal Foams*. Prog. Mater. Sci., **46**, 559–632 (2001).
- Wood J.T., *Production and Applications of Continuously Cast, Foamed Aluminum*. Proc. of Fraunhofer USA Metal Foam Symp., Verlag MIT Publ., 31-35 (1997).

ANALIZA SEM A SPUMELOR METALICE PE BAZĂ DE AlMg CU ADAOS DE SiC

(Rezumat)

Sunt prezentate câteva rezultate legate de cercetarea spumelor metalice bazate pe aliajul metalic AlMg10, obținut prin adăugarea în topitura barbotată cu C_4H_{10} de

particule de SiC. Este analizată microstructura acestor spume prin utilizarea SEM, punându-se în evidență rețeaua de pori interpătrunși, dezvoltată în jurul particulelor de SiC precum și alte aspecte microstructurale caracteristice.

Spuma formată la suprafața topiturii a fost evacuată printr-un dispozitiv special conceput, adaptat la cuptorul respectiv. După răcirea în aer, din spuma obținută s-au prelevat probe, adaptate special pentru studiul metalografic pe microscopul electronic cu baleaj.

BULETINUL INSTITUTULUI POLITEHNIC DIN IAȘI
Publicat de
Universitatea Tehnică „Gheorghe Asachi” din Iași
Tomul LX (LXIV), Fasc. 1-2, 2014
Secția
ȘTIINȚA ȘI INGINERIA MATERIALELOR

HIGH ENTROPY ALLOYS – A NEW WORLD A MATERIALS

BY

GHEORGHE BULUC*, **IULIA FLOREA** and **IOAN CARCEA**

“Gheorghe Asachi” Technical University of Iași
Faculty of Material Science and Engineering

Received: January 14, 2014

Accepted for publication: February 14, 2014

Abstract: Each high-entropy alloy (HEA) contains multiple elements, major and minor elements. The basic principle behind HEAs is that significantly high mixing entropies of solid solution phases enhance their stability as compared with intermetallic compounds, especially at high temperatures. This enhancement allows them to be easily synthesized, processed, analyzed, manipulated, and used. In a broad sense, HEAs are preferentially defined as those alloys containing at least five principal elements, each having the atomic percentage between 5% and 35%. The atomic percentage of each minor element, if any, is hence less than 5%. In this paper we show basic information and some properties of high entropy alloys.

Keywords: high-entropy alloy; hardness tests; SEM analysis.

1. Introduction

High entropy alloys (HEAs), containing five to thirteen metallic elements, with a concentration in the range of 5 to 35 % for each element, exhibit very interesting properties (mechanical, tribological, formability, magnetism) (Yeh *et al.*, 2007). Up to the 1970s, almost all traditional alloys has been developed and provided a wide spectrum of properties and performance. There have been about 30 commonly used traditional alloy systems, including

*Corresponding author: *e-mail*: gheo_u@yahoo.com

steel, aluminium, copper, etc, as depicted, for example, in the ASM Metals Handbooks. However, they were unsatisfactory in many aspects of application (Yeh *et al.*, 2007). Therefore, many efforts have been exerted to develop new metals in the last four decades. In alloys with high entropy will be no element mole fraction greater than 30% so there will be no metal matrix in alloy composition. Studies of high entropy alloys have shown that they have a almost amorphous structure demonstrated by X-ray diffraction and differential scanning calorimetric analysis. HEA has a high atomic disorder with mechanical properties comparable to the glass therefore are brittle (Yeh *et al.*, 2004). The research performed showed that this alloy exhibits high hardness and corrosion resistance and good thermal stability as well. (Yeh *et al.*, 2004; Muscalu *et al.*, 2013). High entropy alloys could have many applications for example: tools, molds, dies, mechanical parts and furnace parts, foundries and marine application for piping and pump components which requires an excellent corrosion resistance, hard and antisticking coating for molds and tools and so on (Yeh *et al.*, 2007).

These alloys were typically composed of one or two principal elements, minor elements being added in order to modify their properties [2, 3]. As elements we can use the main metals: beryllium (Be), magnesium (Mg), aluminum (Al), scandium (Sc), titanium (Ti), vanadium (V), chromium (Cr), manganese (Mn), iron (Fe), cobalt (Co), nickel (Ni), copper (Cu), zinc (Zn), yttrium (Y), zirconium (Zr), niobium (Nb), molybdenum (Mo), ruthenium (Ru), rhodium (Rh), palladium (Pd), silver (Ag), hafnium (Hf), tantalum (Ta), tungsten (W), platinum (Pt), gold (Au), lanthanum (La), cerium (Ce) and so on. Of course in addition to these items we can add minor elements, named like this because their molar fraction in the alloy is lower than 3.5%. In a high entropy alloy, the elements can be metallic or nonmetallic and can be selected from the following elements: lithium, sodium, scandium, titanium, vanadium, chromium, manganese, iron, cobalt, nickel, copper, zinc, gallium, germanium, strontium, yttrium, zirconium, niobium, molybdenum, ruthenium, rhodium, palladium, silver, cadmium, indium, platinum, gold, bismuth, lanthanum metal. Non-metallic elements may be for instance, carbon, boron, silicon, phosphorus, sulfur, hydrogen, oxygen, nitrogen and so on.

2. Melting Techniques

Melting and casting techniques, with equilibrium and nonequilibrium cooling rates, have been used to produce high entropy alloys in the shape of rods, bars, and ribbons. The most popular melt processing techniques are vacuum arc melting, vacuum induction melting, and melt spinning. Mechanical alloying (MA) followed by sintering has been the major solid-state processing route to produce sintered products. Sputtering, plasma nitriding, and cladding are the surface modification techniques used to produce thin films and thick

layers of high entropy alloys on various substrates. A vast majority of high entropy alloys that have been reported so far has been produced by vacuum arc melting and a few by vacuum induction melting. However, the disadvantage of this technique is the possibility of evaporation of certain low-boiling point elements during the alloy preparation thus making compositional control more difficult. In such cases, induction and resistance heating furnaces have been adopted for making the alloys (Cantor *et al.*, 2004; Murty *et al.*, 2014).

The high entropy alloys obtained by powder metallurgy route need to be sintered to achieve dense components. Conventional sintering of nanocrystalline alloy powders can lead to significant grain growth during the exposure of the alloy powders to high temperatures for long periods. In order to avoid this, nanocrystalline alloys obtained by MA are usually consolidated by spark plasma sintering (SPS). SPS involves application of high amperage pulsed current (up to 5,000 A) through the sample kept usually in a graphite die, while simultaneously applying pressures to the tune of about 100 MPa⁶ (Cantor *et al.*, 2004; Murty *et al.*, 2014).

3. Experimental Procedures

Upon researching these methods we developed high entropy alloy FeNiCrCuAl, using induction melt method. For the preparation of this alloy an 8,000 Hz medium frequency induction furnace was used (Fig.1).



Fig. 1 – Induction heating furnace of medium frequency 8,000 Hz.

3.1. Analysis by Scanning Electron Microscope

For microstructural characterization the samples were mechanically processed by grinding and chemical attack with NITAL. For the microstructural characterization we used an electron microscope on LMHII VegaTescan equipment using a secondary electron detector (SE) at a voltage of 30 kV

electron gun. The following figures show the surface microstructures high entropy alloy FeNiCrCuAl for all two samples.

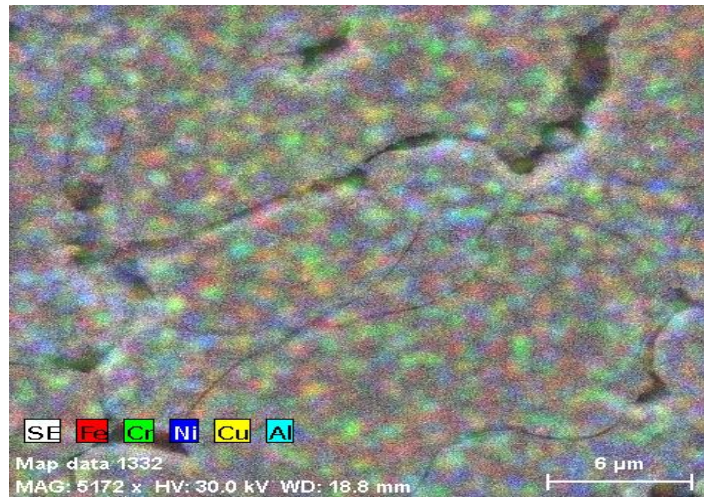


Fig. 2 – The distribution of chemical elements in the alloy with high entropy, FeNiCrCuAl.

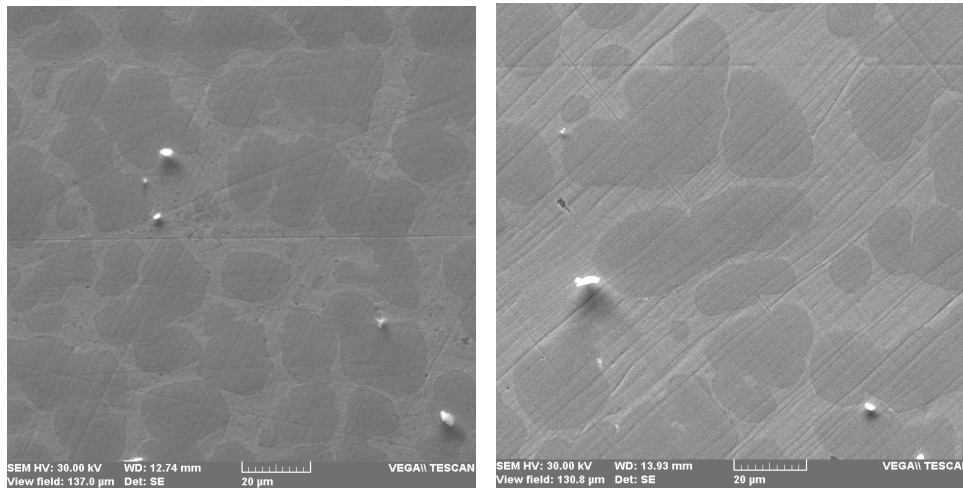


Fig. 3 – Image SEM for sample 1 - A: 500x and B: 1kx

In those pictures we can observe the grain boundaries. The results show that the structure of the alloys is a typical dendritic crystal structure. As Al content increases, the morphology of the microstructure varies and the grains coarsen.

In Table 1, we can observe the hardness values, of high entropy alloys FeNiCrCuAl.

Table 1
Hardness Tests

	Rockwell (HRC)	Vickers (HV)	Brinell
FeNiCrCu	24.1	260	247
FeNiCrCuAl5%	41.2	402	381
FeNiCrCuAl10%	39	382	262

4. Conclusions

The alloy obtained and researched in this paper is FeNiCrCuAl. In conclusion, HEAs and HE-related materials have potential applications in different fields and are expected to replace traditional materials in many sectors. In just a decade from 2004, extraordinary progress has been made. This research theme has caught global attention.

Analyzing the FeNiCrCuAl.alloy by scanning electron microscopy it was observed that the alloy has a FCC structure and exhibits a dendritic morphology after the solidification process.

Further studies are being carried out to investigate the formation mechanism of the oxidation products, high temperature strength and corrosion tests of these alloys.

Acknowledgements. This work was supported by the strategic grant POSDRU/159/1.5/S/133652, co-financed by the European Social Fund within the Sectorial Operational Program Human Resources Development 2007 – 2013.

REFERENCES

- Cantor B., Chang I., Knight P., Vincent A., *Microstructural Development in Equiatomic Multicomponent Alloy*. Mater. Sci. Eng., **A**, 375-377 (2004).
- Guo N., Sun H., Gao P., *et al.*, *Effect of the Number of Principal Elements on Microstructure and Performance of High-entropy with Multi-principal Elements*. New Technology & New Process, **6**, 87-91 (2013).
- Murty B.S., Yeh J.W., Ranganthan S., *High Entropy Alloys*. 77-80, 91-115 (2014).
- Muscalu I., Bălătescu O., Florea R.M., Soare V., Chelariu R., Carcea I., *High Entropy Alloys*. JOAM, **15**, 7- 8, 761-767 (2013).
- Ren M.X., Li B.S., *Phase Analysis of CrFeCoNiCu High Entropy Alloy*. J. of Mater. Engng., **24** (2012).
- Varalakshmi S., Kamaraj M., Murty B.S., *Synthesis and Characterization of Nanocrystalline AlFeTiCrZnCu High Entropy Solid Solution by Mechanical Alloying*. J. of Alloys and Compounds, **460**, 253-257 (2008).

- Yeh J.W., Chen S.K., Lin S.J., Gan J.Y., Chin T.S., Shun T.T., *et al.*, *Nanostructured High Entropy Alloys with Multiple Principal Elements: Novel Alloy Design Concepts and Outcomes*. Adv. Eng. Mater., **299**, 6 (2004).
- Yeh J.W., Chen S.K., Lin S.L., *et al.*, *Microstructural Control and Properties Optimization of High Entropy Alloys*. Adv. Eng. Mater., **6** (2004).
- Yeh, J.W., Chen Y.L., Jien S., *High Entropy Alloys – A New Area of Exploration*. Mater. Sci., **560**, 1-9 (2007).
- Zhang L. S., Ma G.L., Fu L. C., Tian J., *Recent Progress in High-entropy Alloy*. Adv. Mater., **631-632**, (2013).

ALIAJE CU ENTROPIE RIDICATĂ – O NOUĂ LUME A MATERIALELOR

(Rezumat)

Fiecare aliaj cu entropie ridicată conține multiple elemente, elemente principale sau minore. Principiul de bază pentru aliajele cu entropie ridicată este entropia mare de amestec a fazelor tip soluție solidă, care mărește stabilitatea lor în comparație cu compușii intermetalici, în special la temperaturi ridicate. Această creștere de entropie permite obținerea, analiza, procesarea și utilizarea lor accesibilă. Cu alte cuvinte, domeniul aliajelor cu entropie ridicată este definit ca: aliaje care conțin cel puțin cinci elemente principale (majoritare), fiecare având un procentaj atomic cuprins între 5 și 35%. Procentajul atomic al fiecărui element atomic secundar (minoritar), dacă există, este mai mic de 5%. În această lucrare sunt prezentate informații de bază și câteva proprietăți ale aliajelor cu entropie ridicată.

BULETINUL INSTITUTULUI POLITEHNIC DIN IAȘI
Publicat de
Universitatea Tehnică „Gheorghe Asachi” din Iași
Tomul LX (LXIV), Fasc. 1-2, 2014
Secția
ȘTIINȚA ȘI INGINERIA MATERIALELOR

STUDIES REGARDING THE ADHERENCE OF THE ELECTRO- SPARK DEPOSITION COATING LAYER ON THE HEAT TREATED LOW ALLOY STEEL SUPPORT

BY

MANUELA-CRISTINA PERJU*, CARMEN NEJNERU,
MIHAI AXINTE and CĂTĂLIN-ANDREI ȚUGUI

“Gheorghe Asachi” Technical University of Iași
Faculty of Material Science and Engineering

Received: January 16, 2014

Accepted for publication: February 28, 2014

Abstract: The purpose of this paper is to analyze the adherence between the deposited layer and the base material (mild steel). The deposition is realized using pulsed electrical discharge method, on a heat treated steel (martensitic quenching and tempering low). Deposited layer adherence will be studied by studying the layer cracking behavior of the tensile test specimens. Depending on the technological properties of the deposited material substrate it will create an interface area with different dimensions and physical-technological properties.

Keywords: test tensile; steel; electro-spark deposition; interface; layer adhesion.

1. Introduction

The machine building industry is one of the major consumers of material, in particular metal material.

Competition in this field, the technical process and imposed requirements, asks for good knowledge of material properties, development of

*Corresponding author: *e-mail*: cryss_ela@yahoo.com

new materials, treatments and processing technologies to ensure operational requirements at minimum cost (Perju *et al.*, 2013).

Steels used for parts which are in relative motion and contact with other parts must ensure high toughness core characteristics, while exterior areas should provide good resistance to wear. Such characteristics can be obtained by heat treatment or by coating the surface by thermo-chemical treatments using a variety of methods.

One of these deposition methods is pulsed electrical discharge method. On impact with the base material surface, the particles of molten metal from the electrode flatten, breaks and anchors the substrate, forming a metallic layer. Due to the high roughness the layers are sometimes subject to grinding, this operation requiring a very good adherence to the substrate layer.

Obtaining thin films with special properties (wear resistance, corrosion resistance and impact resistance) requires a correct choice of filler material in strict correlation with the physical and mechanical properties of the support material (Liu Jun *et al.*, 2005).

Adherence of the pulsed electrical discharge deposited layer depends on the nature of the electrode and the base material (chemical composition, austenitic grain size, mechanical properties (elongation, σ_c , σ_r , KCU, Rm) (Perju *et al.*, 2013).

2. Methods and materials

We used the electro-spark deposition method. The technology can be defined as a micro-welding in pulses, enabling deposition for the "electrode material" on a metal substrate by mass transport, performed at high intensity current and short periods of time (Alexandru & Strugaru, 2008; Liu Jun *et al.*, 2005; Vermeşan *et al.*, 1999).

The deposition was made with the Elitron 22A installation, surface characteristics analysis was made with scanning electron microscope (SEM), and chemical analysis for the surface layer was made with EDX sensor (Energy Dispersive X-Ray).

For the experiment was used C 15, (DIN 1.0401) laminated bar. This is a high quality carbon steel with a low carbon content, also called case-hardening steel, whose chemical composition is shown in Table 1 (Alexandru *et al.*, 1997), determined by spectrometer Foundry Master.

Table 1
Chemical composition for C 15, [%]

Fe	C	Mn	Si	S	P	Cr	Ni	Other
99.1	0.162	0.302	0.107	0.0275	0.0101	0.0613	0.0411	Balance

Specimens were made, whose dimensions can be seen in Fig.1. The specimens have tensile testing standard shape for metal sheets.

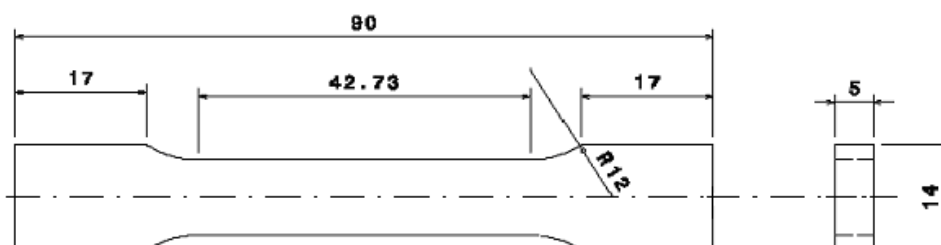


Fig. 1 – Tensile stress specimen for metal sheets.

3. Results and Discussions

The primary means for highlighting the strength capacity is the heat treatment of steels, properly applied to their chemical composition and the considered part type. Corresponding behavior to the heat treatment and, especially reproducibility characteristics, obtained in compliance with the same thermal parameters (time, temperature, etc.), can be achieved only in the case of a quality steel, with lower levels of residues and inclusions, developed according to specific technologies for this purpose.

The hardening heat treatment, carried out in an oven with SiC bars consisted of heating the test specimens at $T = 900^{\circ}\text{C}$, maintaining $\frac{1}{2}$ h, followed by cooling in water. Low tempering treatment, achieved in a SiC bars furnace, consisted of heating the test specimens at $T = 180^{\circ}\text{C}$, maintaining 3 h, followed by cooling in air.

Quenching C 15 steel, is not the proper label, because its completion does not obtains martensite structure but has as effect a relative hardening by changing the P and Fa phases ratio, to a pearlite increased quantity. In this manner the suddenly cooling, leads to obtaining a pearlitic structure out of balance (lower carbon quantity pearlite, but a higher quantity, which leads to a tougher material). The low tempering has the effect of obtaining a stabilized structure after quenching.

We achieved thin layer coatings by pulsed electric discharge method, (Liu Dongyan *et al.*, 2007; Vermeşan *et al.*, 1999), in order to modify the surface properties for the base material, steel C 15, both for the laminated sample, also the heat treated samples. Titanium and tungsten was the metal filler that we have been used as electrodes (Chen Zheng & Zhou, 2006a, 2006b; Cheng Luo *et al.*, 2008; Wang Ruijun *et al.*, 2005). Taking into account that the main objective is to improve the wear behavior by deposition of hard layers, it appears to be necessary, in order to achieve the objective of multilayer surfaces generation: comparable properties of the anchor layer with the support material and coating surface with required properties.

Tensile tests were performed on rectangular laminated control on machine tester Instron 3382. Tensile tests were performed both until breaking the specimen and until the bottleneck. For the control test samples one type of tests were made: a tensile test (complete with broken specimen).

3.1. Macroscopic Analysis of Laminated and Heat Treated Specimens after Tensile Testing

Fracture macro photos were studied, and were observed striations and longitudinal cracks in the direction of drawing, which shows great adhesion with the substrate, acting as a microalloyed area.

The pulling force was large enough, if not so, the layer-substrate adhesion bonds were weak and the coating would be peeled off.

Sample macrostructure (Fig. 2), quenched and high tempered, coated by pulsed electrical discharge method shows a breaking fracture similar to a semi-soft material (slightly hardened), with elongated grains on the break section, but with an elongation less pronounced than in the annealed sample.

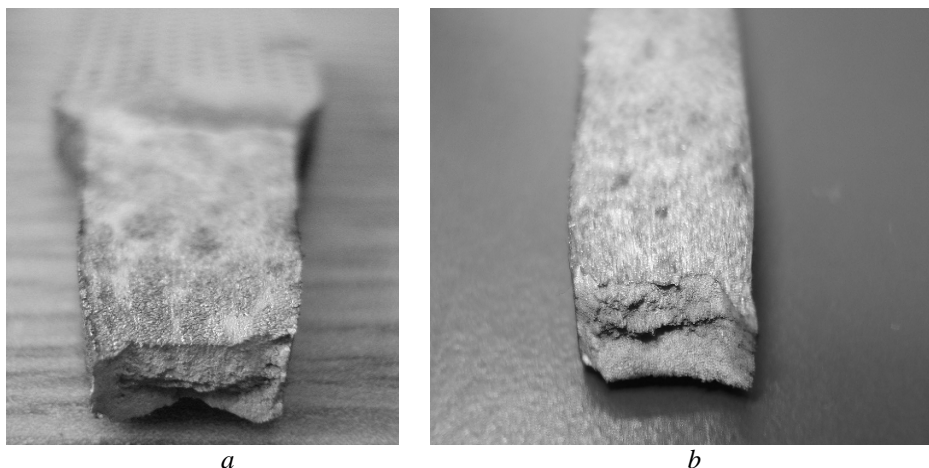


Fig. 2 – Fracture images for the tensile tested coated samples: *a* – laminated sample; *b* – heat treated sample.

3.2. SEM Analysis of the Tensile Breaking Tested Specimens

When testing leads to the tensile breaking, the characteristics σ - ϵ measured parameters are presented in Table 2.

SEM analysis for C 15 steel fracture, coated with complex carbide of W and Ti, quenched and high tempered, shows that the coating layer is well anchored into the substrate layer (Fig. 4). The elastic modulus, yield strength and ultimate yield are closer comparing to the annealed steel, which can be seen into the microcracks that appear into the coating layer and into the substrate.

The quenched and tempered substrate is medium-hard and presents a good consistency with the W and Ti coating layer, which increases the wearing behavior properties.

The coating layer thickness is between 20...30 μm , and the surface is slightly bumpy due to the partially melted drops, embedded in the base material (Fig. 4 c). Initiation of microcracks is located in the confluence of droplets or other defects, as well as material overlapping, adherences, etc. EDX analysis for the coating layer shows a 34% W component, 38% Fe, 8% Ti, and 13% C in immediate vicinity of the surface. Due to the massive presence of the deposited tungsten, the layer is rough and due to the titanium presence, which has the 22 atomic number, close to the 26 for Fe, the layer adheres well to the substrate due to the compatibility the chemical elements.

Table 2
The Values for Sample Breaking Tensile Testing

Characteristic curve σ - ϵ for C 15 steel	The maximum force, [N]	Breaking strain ϵ_r , [%]	Elastic modulus E , [MPa]
	32,863.62	18.96	7,275.33
Ultimate yield σ_r , [MPa]	Yield strength σ_c , [MPa]	Yield strain ϵ_c , [%]	
656.73218	458.60	6.24478	

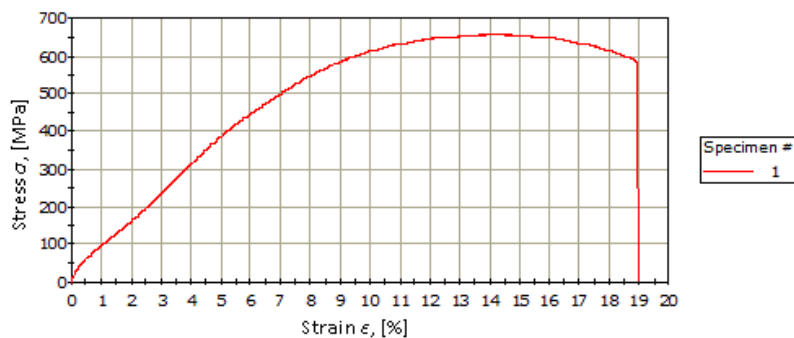


Fig. 3 – Tensile test specimen to failure.

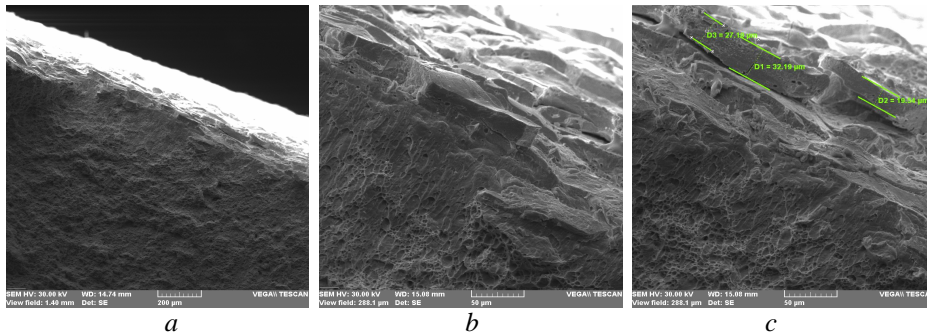


Fig. 4 – SEM microstructures: a – 200 μm ; b – 50 μm ; c – 50 μm .

Tungsten is an element with a big atomic number, which does not enhance the alloying with the base material.

3.3. Analysis of the Strain Characteristics for Layer-Substrate, Depending on the Strength and Plasticity Characteristics, Measures by Tensile Test

During functional loading for thin film coated parts by electrical discharge pulse method, the strain state presents much more interest than the stress state. The substrate state, influence the characteristic curve (σ - ϵ), meaning by default the yield point, ultimate yield and elastic modulus.

The coated layer presents a yield point, ultimate yield and elastic modulus, characteristic for the composing elements for deposition electrode. There are not overlapping with the base material characteristics, meaning that the coated layer and the support substrate do not get in the plastic domain at the same time, and the ultimate strength varies.

Generally, depositions are made in order to enhance the wear and/or corrosion resistance, which makes that the coated layer is much tougher than the substrate, with lower elastic properties, and the cracks are much quicker initiated in the coating than the substrate.

Giving a certain stress, which produces a certain strain ϵ_a , in the case of the coated annealed sample, the deposited layer is still in the elastic domain, while the steel is in the plastic domain.

This means that are residual strains, partially independent from the interface, which recovers after stress is relieved, due to the fact that its domain has not crosses the elastic domain, into the plastic one.

In the case of the quenched and tempered steel, at the same stress, which creates the ϵ_a strain, the submitted layer and the substrate material are both in the elastic domain, and the stress do not cause cracks into the sample.

The study had two objectives:

a) to analyze the tensile behavior of the layer-substrate subassembly when using the base material which is subject to various heat treatments (different technological properties);

b) to analyze the adherence of the deposited layer on to the base material, previously annealed, quenched and low tempered, for the tensile test part.

4. Conclusion

Dangerous stresses are stretching in layer because it creates prerequisites occurrence of microcracks which can evolve in exfoliation of the deposited layer.

These analyzes showed that the deposition layer is well anchored in the substrate, due to the propagation of cracks in the drawing direction.

Cracks are evenly distributed, without exfoliation and layer separation, which is due to a good coherence between layer and substrate obtained after microalloying of base material and deposition.

REFERENCES

- Alexandru A., Strugaru S.I., *Alierea și depunerea superficială prin scânteie electrică-Influența tratamentelor termice asupra caracteristicilor straturilor*. Edit. Tehnopress, Iași, 2008.
- Alexandru I., Popovici R., Baciu C., Călin M., Cojocaru V., Bulancea V., Carcea I., Alexandru A., Paloșanu G., *Alegerea și utilizarea materialelor metalice*. Edit. Did. și Pedag., București, 1997.
- Chen Zheng, Zhou Y., *Surface Modification of Resistance Welding Electrode by Electro-Spark Deposited Composite Coatings. Part I. Coating Characterization*. Surface & Coatings Technol., **201**, 1503-1510 (2006a).
- Chen Zheng, Zhou Y., *Surface Modification of Resistance Welding Electrodes by Electro-Spark Deposited Composite Coatings. Part II. Metallurgical Behavior During Welding*. Surface & Coatings Technol., **201**, 2419-2430 (2006b).
- Cheng Luo, Shijie Dong, Xiang Xiong, *Microstructure and Properties of TiC Coating by Vibrating Electrospark Deposition*. Key Engng. Mater., **373-374**, 180-183 (2008).
- Liu Jun, Wang Ruijun, Qian Yiyu, *The Formation Of A Single-Pulse Electrospark Deposition Spot*. Surface & Coatings Technol., **200**, 2433- 2437 (2005).
- Liu Dongyan, Gao Wei, Li Zhengwei, Zhang Haifeng, Hu Zhuangqi, *Electro-Spark Deposition of Fe-Based Amorphous Alloy Coatings*. Mater. Lett., **61**, 165-167 (2007).
- Perju M.-C., Neșneru C., Vizureanu P., Axinte M., Achiței D.-C., *Studies on Layer-Material Interface at Deposition by Impulse Electrical Discharge Method*. The Ann. of "Dunarea de Jos" Univ., Galați, **IX**, Metallurgy a. Mater. Sci., Special Issue, 92-96 (2013).
- Vermeșan G., Vermeșan E., Jichisan-Matiesan D., Cretu A., Negrea G., Vermeșan H., Vlad M., *Introducere în ingineria suprafețelor*. Edit. Dacia, Cluj-Napoca, 1999.
- Wang Ruijun, Qian Yiyu, Liu Jun, *Interface Behavior Study of WC92-Co8 Coating Produced by Electrospark Deposition*. Appl. Surface Sci., **240**, 42-47 (2005).
- * * *Instalație Elitron 22*. Acad. de Științe, Republica Moldova, Chișinău, 1992.

STUDII ASUPRA ADERENȚEI STRATURILOR CU DEPUNERE PRIN DESCĂRCARE ELECTRICĂ ÎN IMPULS PE SUPORT DE OȚEL SLAB ALIAT

(Rezumat)

Se analizează aderența între stratul depus și materialul de bază (oțel slab aliat). Depunerea este realizată folosind metoda descărcării electrice în impuls, pe un oțel tratat termic (călire martensitică și revenire joasă). Aderența stratului depus va fi

studiată prin analiza comportamentului la fisurare a stratului depus pe epruvete încercate la tracțiune. În funcție de proprietățile tehnologice ale substratului materialului depus se va crea o zonă de interfață cu diferite dimensiuni și proprietățile fizico-tehnologice.

BULETINUL INSTITUTULUI POLITEHNIC DIN IAȘI

Publicat de

Universitatea Tehnică „Gheorghe Asachi” din Iași

Tomul LX (LXIV), Fasc. 1-2, 2014

Secția

ȘTIINȚA ȘI INGINERIA MATERIALELOR

IRON WHITENING WHEN MANUFACTURING GREY CAST IRON IN SMALL AMOUNT

BY

VASILE COJOCARU-FILIPCIUC*

“Gheorghe Asachi” Technical University of Iași

Faculty of Material Science and Engineering

Received: February 17, 2014

Accepted for publication: March 10, 2014

Abstract: In this paper it is analyzed why, when grey cast iron is manufactured by electric induction furnace, in small amount (under 10 kg), in circumstances where metallic charge is formed from grey pig iron, only (having small content of sulfur), without graphitizant modification, even for small degree of overheating in liquid state, grey cast iron is obtained white one. Purpose of the non-metallic inclusions and purpose of remanent graphite for crystallization are analyzed.

Keywords: heterogeneous crystallization; non-metallic inclusions; pure metallic charge; absence of graphitizant modification.

1. Introduction

Factors which determine iron whitening, iron solidification according to the metastable system Fe-Cementite, are the following: cooling rate, maintain time in liquid state, degree of purity, content of antigraphitizant chemical elements, graphitizant modification absence, physic-mechanical treatments, inoculation, degree of overheating in liquid state, etc., factors acting directly or by other parameters, as cooling module (equivalent cooling), castings

**e-mail:* cojocaru52@yahoo.com

configuration, mould kind, pouring temperature, etc. (Sofroni, 1975; Sofroni *et al.*, 1985).

During manufacture, after temperature of metallic bath exceeded liquidus line temperature, the phenomenon of dissolution of remanent graphite and non-metallic inclusions begins.

If metallic charge is formed from metallic sorts only, these ones being grey iron, in all cases, unoverheating liquid iron contains remanent graphite.

Amount of non-metallic inclusions from the unoverheating liquid iron depends of metallic sorts kind.

During melting stage, dissolution phenomenon of remanent graphite and non-metallic inclusions begins in liquid microvolumes that arise.

After all metallic charge is liquid state, dissolution phenomenon of remanent graphite and non-metallic inclusions is conditioned by the metallic bath temperature, non-metallic inclusions kind and time.

Dissolution phenomenon of non-metallic inclusions means development of reactions of dissociation, (1) type and, then, chemical elements diffusion in the solvent which is liquid iron.



where: A and B represent chemical elements.

Development of (1) reaction means breaking of the chemical bounds among component particles either as atoms or the ions.

A reaction (1) type is a topochemical and has three periods – incubation, autoacceleration and reaction average front period.

More, if the non-metallic inclusion is complex, necessary time to complex non-metallic inclusion dissolution is higher because a lot of phenomena occur, such as following: dissolution of complex anion, molecules desorption, appearance of new phases, diffusion processes, etc. (Oprea *et al.*, 1978).

Consequence is that if non-metallic inclusions have large size, these ones will need a higher time for dissolution in liquid metallic matrix.

Non-metallic inclusions can be exogenously and endogenously, those endogenously have negative influence on iron crystallization if they there are in metallic matrix at beginning of iron crystallization.

2. Experiment and Results

It was used for the metallic charge grey pig iron with the following chemical composition: C = 4.2%; Si = 2.6%; Mn = 0.8%; P = 0.12%; S = 0.06%; Fe = balance.

Metallic charge mass was of 5.9 kg.

Fig. 1 represents structure of grey pig iron that was used for charge of the electric induction furnace of 15 kg capacity (furnace capacity was limited by utilization of a melting pot of SiC that was introduced in granulous refractory lining of quartzite). We see that graphite is flake.

Fig. 2 represents structure of manufactured iron after iron was overheated in liquid state at a temperature about 1,300°C and was poured as a casting like that from Fig. 3. One sees in Fig. 2 that iron is white – there is a large number of eutectic austenite separations.

Fig. 4 represents structure of manufactured iron after iron was overheated in liquid state at a temperature about 1500°C. Analyzed sample was taken from the riser of a casting and has diameter of 20 mm. One sees in Fig. 4 that iron is white and eutectic austenite separations were no so many.



Fig. 1 – Structure of grey pig iron used for manufacture. X 48,8 (sample unprocessed by chemical reactive).

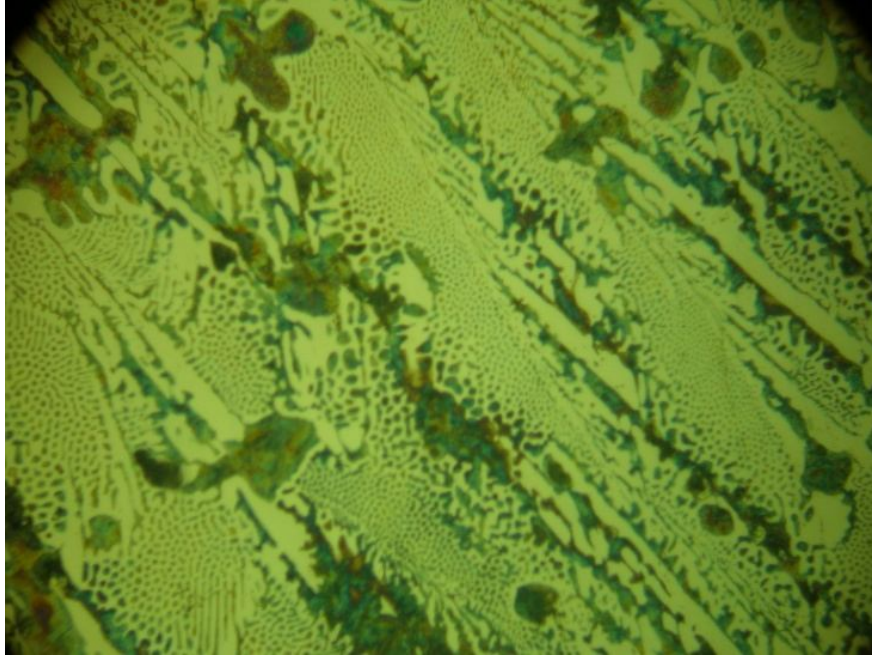


Fig. 2 – Structure of manufactured iron that was overheated in liquid state at temperature about 1,300°C. X 128. (sample processed by chemical reactive).

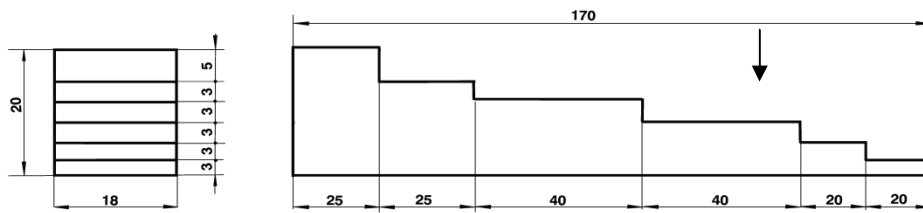


Fig. 3 – Casting used for structure analysis of iron that was overheated in liquid state at temperature about 1,300°C.



Fig. 4 – Structure of manufactured iron that was overheated in liquid state at temperature of about 1,500°C. X 128 (sample processed by chemical reactive).

In consequence, obtained iron was white in both cases-for those two overheating temperatures.

Maintaining time in liquid state, for both overheating temperatures, was about 3 min.

3. Discussion

Presence of endogenously non-metallic inclusions in liquid iron when iron is evacuated from the furnace, is directly related to how the crystallization of iron.

The crystallographic lattice of the non-metallic inclusions is very important. So, if that one is compact (compact hexagonal and compact cubic), chemical elements around them can not diffuse to their inside. Diffusion of the carbon particles to the non-metallic inclusions from metallic bath is very important. This diffusion process is more significant as there is a higher thermodynamic activity gradient of carbon between metallic matrix and non-metallic inclusions that have compact crystallographic lattice. Source [4] shows that around non-metallic inclusions whose crystallographic lattice is compact, there are conditions of graphite growth, the non-metallic inclusions shape dictating graphite shape obtained.

According to source [5], SiO_2 , FeS, SiC, NiS and CaMg represent hexagonal crystallographic system and CaO, MgO, SrO, BaO, MnO, FeO, CeO_2 , Li_2O , TiN, ZrN, Mg_2S , Ni_3S , TeSn, CaS, Ni_2Si , SiS, BaS, MnS, Li_2S , TiC, ZrC and MgS represent cubic crystallographic system.

Presence of chemical compounds that are not carbides or do not contain carbon and that have compact crystallographic system (hexagonal or cubic), in liquid iron when liquid iron is evacuated from the furnace, do that iron to crystallize by metastable system – do not crystallize as white iron. In a situation like this one, degree of undercooling of iron at eutectic transformation is increased. Heterogeneous crystallization is very important for crystallizing in the case of iron.

If the crystallographic lattice of non-metallic inclusions is not compact and non-metallic inclusions do not contain carbon, carbon atoms diffuse in those non-metallic inclusions according to the chemical equilibrium law between two phases. So, carbon thermodynamic activity gradient is increased and, so, it is not possible germination of graphite in the interface between metallic matrix and non-metallic inclusion. In this case, iron has conditions to crystallize by metastable system.

Presence of non-metallic inclusions increases as probability if the metallic charge is heterogeneous and contains a large amount of iron waste.

In the case of this experiment, the metallic charge was formed from grey pig iron, only, ie a metallic sort with a relative large degree of purity. So, for small overheating degrees, liquid iron had not non-metallic inclusions, which meant that heterogeneous crystallization was out of its role.

In addition, pig iron contented a little sulfur content – 0.06%. In this case, coarse inclusions of graphite were dissolved in liquid metallic matrix though overheating degree in liquid state was small (when the sulphur content is large, mostly, graphite lamellae from liquid iron have sulphur particles adsorbed; even one needs temperatures more then 1,500°C for graphite to dissolve in liquid metallic matrix).

Manufacture conditions from the experiment, without graphitizant modification, determined that iron to solidify by metastable system.

4. Conclusions

In the case when one propose manufacture of a small amount of grey iron, non-alloy one, for example, under 10 kg, and metallic charge is formed from grey pig iron that has a small sulphur content or is formed from pig iron of high purity, it is necessary graphitizant modification of iron, classically, with, for example, FeSi75, for whitening avoidance.

REFERENCES

- Cojocaru-Filipiuc V., *Fonte-obținere*. Edit. Samia, Iași, 2003.
Cojocaru-Filipiuc V., *Hypotheses on the Equilibrium of Metallic Materials Based on the Chemical Equilibrium Tendency – Applications for Cast Iron Inoculation*. Edit. Politehniun, Iași, 2011.
Oprea F. *et al.*, *Teoria proceselor metalurgice*. Edit. Did. și Pedag., București, 1978.

Sofroni L. *et al.*, *Turnarea fontei*. Edit. Did. și Pedag., București, 1985.

Sofroni L., *Elaborarea și turnarea aliajelor. Fonte. Oțeluri. Aliaje neferoase*. Edit. Did. și Pedag., București, 1975.

ALBIREA FONTEI ÎN CAZUL ELABORĂRII FONTEI CENUȘII ÎN CANTITATE MICĂ

(Rezumat)

Se analizează de ce, în cazul elaborării fontei în cuptoare electrice cu încălzire prin inducție, în cantitate mică (sub 10 kg), în circumstanțele în care încărcătura metalică este constituită doar din fontă brută cenușie, cu conținut mic de sulf, în absența inoculării (modificării grafitizante), chiar în cazul unor grade mici de supraîncălzire în stare lichidă, aceasta se obține albă. Se face o analiză a rolului jucat de incluziunile nemetalice și de grafitul remanent în cristalizare.

BULETINUL INSTITUTULUI POLITEHNIC DIN IAȘI
Publicat de
Universitatea Tehnică „Gheorghe Asachi” din Iași
Tomul LX (LXIV), Fasc. 1-2, 2014
Secția
ȘTIINȚA ȘI INGINERIA MATERIALELOR

METHOD FOR PRODUCTION OF COMPACTED GRAPHITE CAST IRON

BY

VASILE-COJOCARU FILIPIUC*

“Gheorghe Asachi” Technical University of Iași
Faculty of Material Science and Engineering

Received: February 27, 2014

Accepted for publication: March 20, 2014

Abstract: The theory that was taken into consideration was based on the tendency toward chemical equilibrium for two thermodynamic phases in contact. The determining factor that dictates the form of graphite is interphasic tension between metallic matrix and inoculating agent. So, aluminum is used, mechanically mixed with the inoculating agent, inoculating agent role being getting nodular graphite. Quality of active surface element of aluminium does interphasic tension between metallic matrix and inoculating agent to be small, so that the inoculating agent drop shape to determine getting compacted graphite.

Keywords: compacted graphite; inoculating agent; active surface element; aluminium; mechanical mixture.

1. Introduction

The mechanism of compacted graphite formation is identical to the mechanism of nodular graphite formation, if the inoculating agent is in the liquid state at the iron inoculation temperature.

The decisive factor influencing drop shapes is the value of the interfacial surface tension between the metallic matrix and inoculating agent

**e-mail:* cojocaru52@yahoo.com

drops, σ_{12} , expressed by

$$\sigma_{12} = \sigma_2 - \sigma_1 \cos \theta \sqrt{1 + \left(\frac{\sigma_1 \sin \theta}{\sigma_2 - \sigma_1 \cos \theta} \right)^2}, \quad (1)$$

where: σ_{12} is the interfacial surface tension between the metallic matrix and the drop (phase 1 and phase 2); σ_2 – the interfacial surface tension between the drop and air; σ_1 – the interfacial surface tension between the metallic matrix and air; θ – moistening angle of the drop by the metallic matrix.

The specificity of compacted graphite production consists of achieving compacted shapes for the inoculating agent drops.

The values of σ_{12} interfacial surface tension may be regulated in the following two ways:

- a) by the interventions on the chemical composition of the metallic matrix;
- b) by the interventions on the chemical composition of the inoculating agent.

If the production of spherical drops depended on the absence of surface-active chemical elements in the metallic matrix and in the inoculating agent, the production of drops with compacted shapes depends on the controlled presence of surface-active elements in the metallic matrix and the inoculating agent.

The surface of compacted graphite is bigger than that of nodular graphite, which means that it is more susceptible to dissolution in the metallic matrix. Moreover, the thickness of compacted graphite is inferior to the graphite nodule diameter, which also means shorter dissolution times in the metallic matrix. Therefore, inoculating elements should be adsorbed on the compacted graphite together with the surface-active element or elements, and, hence, they should prevent fast dissolution of compacted graphite (Cojocaru-Filipiuc, 2011).

The surface-active elements must also have the capacity of be adsorbed on graphite, and the adsorption forces must have the same size grade as the inoculating elements.

Fig. 1 is the schematic representation of the mechanism of compacted graphite formation. The term compacted is relative and reference (Ripoşan & Sofroni, 1984) also employs other names for it, such as: vermicular, compacted flaky, semi-ductile, unique, compacted vermicular and vermicular compacted. According to Fig. 1, the carbon particles diffuse from the metallic matrix towards the drops due to the high carbon activity gradient between the metallic matrix and the inoculating agent drops, 1st sequence.

The inoculating agents with densities lower than that of the liquid metallic matrix, at the inoculation temperature, are the most common in industrial practice. Therefore, the graphite nuclei will grow in drops.

Carbon particles diffuse continuously and hence carbon particle agglomerations occur at the metallic matrix-inoculating agent drop interface (2nd sequence).

The sequences marked I, II and III show the maximum contact surface between the metallic matrix and the drops, which is the very surface of the drops.

A higher carbon particle concentration around the drops means a higher molar fraction of carbon and, hence, a higher carbon activity.

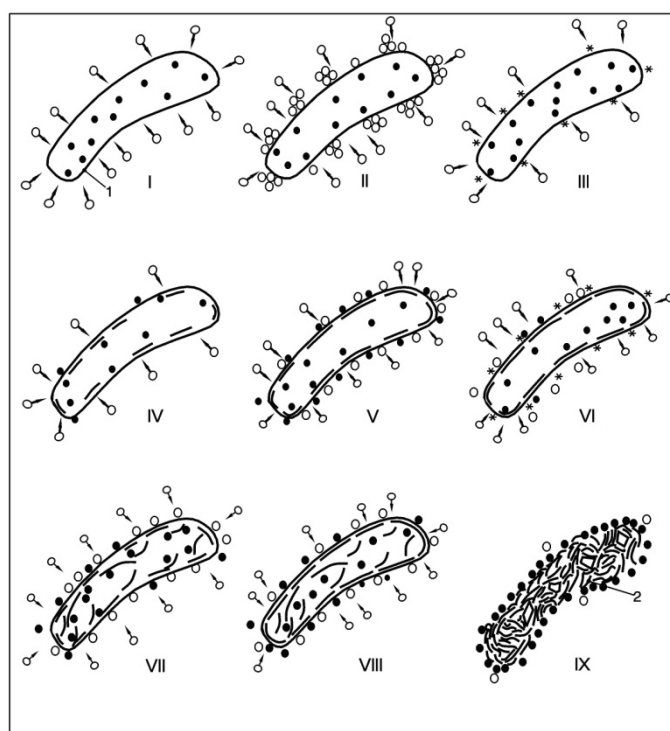


Fig. 1 – Drawing of the mechanism of compacted graphite formation in the inoculating agent drops: ● – inoculating agent atoms and surface-active elements; ○ – carbon particles; /, □ – graphite single crystals; 1 – inoculating agent drops; 2 – crystalline body of compacted graphite; * – graphite nuclei; the white background around the drops is the metallic matrix.

The chemical composition of the metallic matrix must ensure the highest possible carbon activity, which should be as close to 1 as possible. For instance, this is achieved in practice for little hypoeutectic, eutectic and hypereutectic irons.

Carbon activity reaches 1 due to the carbon concentration increase and

the carbon activity coefficient increase caused by the decrease of the temperature of the metallic matrix. Hence, hexagonal graphite nuclei are formed in the interface area – 3rd sequence –, where the graphite nuclei are marked by asterisks.

The graphite nuclei start to grow in drops, since the carbon particles diffuse continuously.

The contact surface between the metallic matrix and the drops (4th sequence) decreases with the increase of the graphite single crystals, and it becomes minimal when the junction between the graphite single crystals is done, 5th sequence.

A graphite single crystal is a phase, which means that there no longer is a direct contact between the metallic matrix and the drops around it, and therefore there is no carbon activity gradient between the two phases (metallic matrix and drops). Hence, the carbon particles stop diffusing. On the other hand, there is a direct contact between the metallic matrix and the drops where the junctions between the graphite single crystals occur, and where the process of carbon particle diffusion continues and generates new graphite nuclei, 6th sequence.

When the graphite single crystals grow, the inoculating agent particles and the surface-active element particles diffuse outside the drops, in the interface area.

The surface-active element particles have the specific capacity of gathering in the interface area; however, at the same time, some surface-active elements also have different capacities of dissolving in the metallic matrix. Hence, one may conclude that the surface-active elements included in the chemical composition of the inoculating agents should not dissolve in the metallic matrix that is in Fe. Yet, if the dissolution does occur, the saturation point should be very low. This requirement is accounted for by the need of the surface-active elements to remain in the metallic matrix-drop interface, so that, in the end, after the completion of the crystalline bodies of graphite, the surface-active elements in the interface and the inoculating agent particles would be adsorbed on the crystalline bodies of graphite, thus significantly delaying their dissolution in the metallic matrix.

For both compacted graphite and graphite nodule formation, emphasis is laid on the major role played by the silicon in the inoculating agent that diffuses in the metallic matrix, around the inoculating agent drops, in order to enhance carbon activity. The important role played by the iron in the inoculating agent is also underlined, as it increases the drop density and it does not diffuse in the metallic matrix due to the negative activity gradient (the iron activity in the metallic matrix is higher than the iron activity in the inoculating agent drops).

The new graphite nuclei formed in the interstices between the graphite single crystals in the first single crystal layer start to grow in the inoculating agent drops, which determines the mechanical impact between the growing graphite single crystals and the graphite single crystals in the first layer. That mechanical impact materializes in the dislocation of graphite single crystals found in the first layer and their directing towards the middle of the drops. The inoculating agent particles diffuse towards the outside of the drops during graphite single crystal dislocation, while the contact surface between the metallic matrix and the inoculating agent drops increases, 7th sequence. The carbon particle diffusion flow from the metallic matrix towards the inoculating agent drops is thus increased, and the growth of the graphite single crystals found in the second layer is also enhanced. This is followed by the junction between the graphite single crystals, 7th sequence. The formation of new graphite nuclei and their growth as single crystals are repeated until the inoculating agent drops are “filled” with graphite single crystals, 9th sequence. The 9th sequence shows that all the inoculating agent particles (the inoculating chemical elements and the surface-active chemical elements) are in the metallic matrix-compacted graphite interface.

Adsorption bonds are established between the inoculating chemical elements and the surface-active chemical elements, on the one hand, and the compacted graphite inclusions, on the other hand, which are designed to delay the dissolution of the compacted graphite inclusions in the liquid metallic matrix.

2. Experiment and results

One proposes experimenting of a new method of obtaining for compacted graphite cast iron, by inoculation.

Concretely, FeSiCaMg inoculating agent (9.5%Mg; 45%Si; 1.5% Ca; 44% Fe), having granulation of 2...6 mm, of 1% amount, by mechanical mixture with Al as pieces of sheet whose thickness is of 1 mm, of the same size like that of the inoculating agent pieces and of 0.5% amount is used for inoculation of iron 6.5 kg with the following chemical composition: 4.2%C; 3% Si; 0.8%Mn; 0.12%P; 0.06%S; balance for Fe (the Si content was increased to 3% concentration for significant increasing of the carbon thermodynamic activity in the liquid iron). Iron was manufactured in an electric induction furnace – melting pot of 20 kg capacity.

In Fig. 2 it is presented structure of the pig iron that was used in metallic charge and in Fig. 3 it is presented structure of compacted graphite cast iron obtained by inoculation, according to original method previously presented.



Fig. 2 – Structure of pig iron used in charge of the furnace. X 48.8.

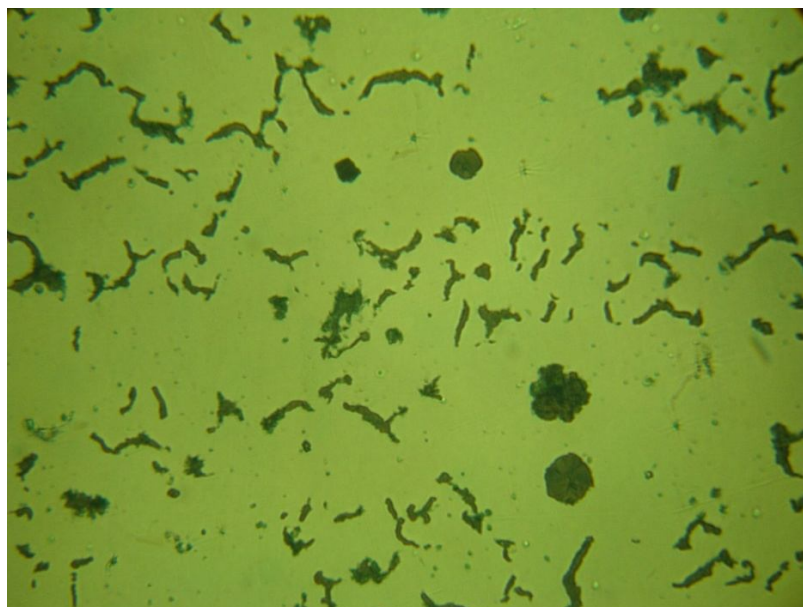


Fig. 3 – Structure of compacted graphite cast iron obtained by new method proposed and experimented for this paper. X 128.

3. Discussion

Compacted graphite cast iron is routinely obtained by the iron inoculation, using inoculating agents which contain chemical elements that there are in the inoculating agents used for nodular graphite cast iron obtaining and there upon active surface elements are added. Most are found in practice, Ti, (Sergeant & Evans, 1978), Al, (Jukov *et al.*, 1973), Zr, (Barga *et al.*), Al+Zr, (Skrebțov *et al.*, 1981), Ti+Al, (Lalich & La Presta, 1978) and Te. Tybulozuk *et al.*, (1976), shows introducing of Sb in iron proposed to inoculate, Horie, (1977), analyses introducing of As in liquid iron and Campomanes & Goller, (1975), shows that Sb is introduced in bath iron and inoculating agent.

Active surface elements that can be take into consideration for compacted graphite cast iron obtaining are Te, As, Sb, Sn, Al, In, Cd, Ag, Ti, Pb, Bi, Ga, B, N, O, H, S, Se and Cu (Cojocaru-Filipiuc, 2011).

If there are active surface elements in the inoculating agent, these ones are expelled from drops of inoculating agent by the growing of graphite monocrystals in drops and they will be placed to interface between metallic matrix and graphite inclusions. Ideally, active surface elements must be in adsorption state at graphite surface and by great adsorption forces. So, dissolving of graphite inclusions in liquid metallic matrix is delayed.

Inoculating agent that contains active surface elements is obtained by manufacture.

If inoculating agent grains are mixed with pieces of aluminium, grains of inoculating agent being of the same order of magnitude with aluminium pieces, aluminium pieces support the some regimen as the inoculating agent grains.

Aluminium density is small (2.7 g/cm^3) compared to the one of liquid iron (for example, 6.9 g/cm^3), which means eliminating tendency from the metallic both. Inoculating agent density is about 3 g/cm^3 , *i.e.* it is of the some order of magnitude with that one of aluminium.

Therefore, technique of inoculating agent introducing in liquid iron “solves” problem of aluminium distributing in metallic bath as for inoculating agent. So, it obtains presence of aluminium particles near inoculating agent particles and presence of aluminium drops near inoculating agent drops. Here’s how aluminium active surface element has supplementary means to concentrate easier in interface between metallic matrix and inoculating agent drops.

Consequence is transformation of circular drops of inoculating agent to compacted drops.

This method of compacted graphite cast iron obtaining is recommended for obtaining of iron little quantity, such as in spare parts (small batch or unique).

4. Conclusion

Obtaining method of compacted graphite cast iron, which was presented in this paper, is recommended to inoculate small quantities of iron, for obtaining of small batch of castings.

REFERENCES

- Barga F. *et al.*, *Almeneti grafitos öntöttvas eloallitasara alkalmos kezelöangang*. Patent Hungary, No. 166327.
- Campomanes E., Goller R., *Production of Cast Iron Containing Intermediate Forms of Graphite*. AFS Transaction, **83**, 55-62 (1975).
- Cojocaru-Filipiuc V., *Hypotheses on the Production of Metallic Materials based on the Chemical Equilibrium Tendency – Applications for Cast Iron Inoculation*. Edit. Politehniun, Iași, 2011.
- Horie H., *The Inhibition Effects of Arsenic on Spheroidal Graphite Formation in Cast Iron*. Imono, 5, 281-286 (1977).
- Jukov A.A. *et al.*, *Kompleksnâe modifikatorî dlia polucenia leghirovanova ciuguna s şorovidnâm I vermiculiarnâm grafitom*. Liteinoe Proizvodstvo, 6, 17-19 (1973).
- Lalich M.J., La Presta S.J., *Uses of Compacted Graphite Cast Irons*. Foundry Manag. a. Technol., 9, 56-57 (1978).
- Ripoşan I., Sofroni L., *Fonta cu grafit vermicular*. Edit. Tehnică, Bucureşti, 1984.
- Sergeant G.F., Evans E.R., *The Production and Properties of Compacted Graphite Irons*. The British Foundryman, 5, 115-124 (1978).
- Skrebţov A.M. *et al.*, *Regulirovanie svoistv vâsokoprocinovo ciuguna modifikatorami raznovo sostava*. Liteinoe Proizvodstvo, 1, 30-31 (1981).
- Tybulozuk J. *et al.*, *Etude sur les formes dégénérée du graphite en vue du controle magnetique des pieces moulees en fontes à graphite spheroidal*. Fonderie, 35, 123-138 (1976).

METODĂ DE PRODUCERE A FONTEI CU GRAFIT COMPACTIZAT

(Rezumat)

Teoria luată în consideraţie se bazează pe tendinţa spre echilibrul chimic a două faze termodinamice aflate în contact. Factorul determinant care dictează forma grafitului este tensiunea interfaţică matrice metalică–modificator. Astfel, se utilizează aluminiul, în amestec mecanic cu modificatorul ce are ca rol obţinerea fontei cu grafit nodular. Calitatea de element superficial active a aluminiului face ca tensiunea interfaţică matrice metalică–modificator să se micşoreze, așa încât forma picăturii de modificator să determine obţinerea grafitului compactizat.

BULETINUL INSTITUTULUI POLITEHNIC DIN IAȘI
Publicat de
Universitatea Tehnică „Gheorghe Asachi” din Iași
Tomul LX (LXIV), Fasc. 1-2, 2014
Secția
ȘTIINȚA ȘI INGINERIA MATERIALELOR

NODULAR GRAPHITE OBTAINING MECHANISM, BY MODIFICATION, FOR A TECHNICAL IRON, BY A LIQUID INOCULATING AGENT AT THE INOCULATING TEMPERATURE

BY

VASILE-COJOCARU FILIPIUC* and DANIELA-LUCIA CHICET

“Gheorghe Asachi” Technical University of Iași
Faculty of Material Science and Engineering

Received: March 10, 2014

Accepted for publication: March 28, 2014

Abstract: One presents iron inoculating scheme when inoculating agent is as drops in liquid iron. The scheme is based on the thermodynamic equilibrium law that is established between phases that are in contact. Experiment confirms the filling of the drops of inoculating agents with graphite monocrystals as foils. Experiment confirms inoculating scheme. Investigation is done at an electronic microscope Quanta 200 3-D ($\times 4,000$).

Keywords: tendency to the chemical equilibrium; carbon thermodynamic activity; inoculating agent; graphite monocrystals; graphite nodules.

1. Introduction

Alloy inoculation means formation, artificially, in a metallic matrix – phase 1 from Fig. 1, of a thermodynamic phase – phase 2 from Fig. 1, at the inoculating temperature, as one of the state of aggregation as follows: gaseous, liquid and solid.

Phase 2 represents inoculating agent.

*Corresponding author: *e-mail*: cojocaru52@yahoo.com

One accepts metallic matrix formed from chemical elements E_i , ($i = 1, 2, 3, 4, 5, \dots$), where E_1 is basic chemical element, E_2 is chemical element that has a large diffusion coefficient and E_3, E_4, E_5, \dots represent accompanying chemical elements (Cojocaru-Filipiuc, 2007, 2011).

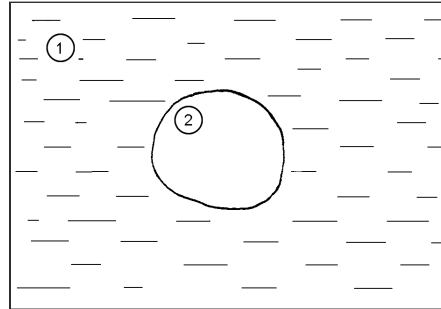


Fig.1 – Drawing of a metallic system made up of two phases: 1 – liquid metallic matrix; 2 – new phase.

In the case of iron, E_1 represents iron, E_2 represents carbon and E_3, E_4, E_5, \dots represent silicon, phosphorus, sulfur, etc.

Phase 2 is formed from chemical elements F_j , ($j = 1, 2, 3 \dots$).

Creation of phases 2 in metallic matrix triggers E_2 element diffusion to phase 2 where is not dissolved.

Phase 2 contents inoculant chemical element (this one must not dissolve in the metallic matrix), necessarily, one or more, and chemical elements having different roles, as thermodynamic activity carbon increase from metallic matrix, (for example, silicon), inoculating agent drops density increase (for example, iron), etc.

When phase 2 is filled with monocrystals of E_2 elements, it is transformed in phase 3, where E_2 element thermodynamic activity becomes 1. So, dissolution phenomenon of phase 3 in metallic matrix begins. This one requires that solidification to begin as soon as possible or that inoculating agent to contain chemical elements that to adsorb at phase 3 surface and with large adsorption forces, what prevents, temporarily, phase 3 dissolution.

2. Inoculation Scheme

Fig. 2 shows how E_2 single crystals are formed and grow in an F_j drop.

The amount of E_2 particles present in the metallic matrix must ensure the formation of the new phase, *i.e.* of phase 3.

In order for the diffusion rate of the chemical element E_2 through the metallic matrix to be high, the activity gradient of element E_2 should be high, which requires a higher E_2 concentration in the metallic matrix and no element E_2 in phase 2.

Once the phase 2 drops are formed in the metallic matrix, the E_2 particle diffusion phenomenon is triggered, from the metallic matrix towards the phase 2 drops.

The high diffusion coefficient should cause the E_2 particle detachment from the other chemical elements E_i in solvent E_1 .

In Fig. 2, the E_2 particles are symbolized by little circles.

The 1st sequence in Fig. 2 shows the E_2 particles and the direction in which they diffuse, symbolized by arrows, as well as the F_j particles, symbolized by full circles. The phase 2 drop is symbolized by a sphere.

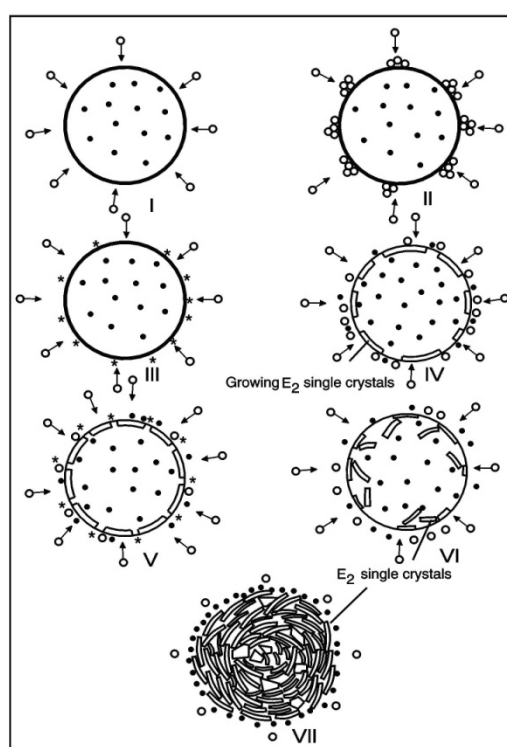


Fig. 2 – Drawing of E_2 single crystal formation and growth. \circ – E_2 particles; \bullet – F_j particles; * – E_2 nuclei. The white background around phases 2 and 3 is the metallic matrix.

If the E_2 particles are atoms, the E_2 atoms diffuse towards the F_j drops, given the tendency to chemical equilibrium.

The E_2 atoms do not get into the phase 2 drops since phases 1 and 2 are immiscible.

The E_2 atom diffusion process is continuous, as long as there is an activity gradient of the element E_2 between phases 1 and 2.

E_2 atom agglomerations occur at the metallic matrix-drop interface, which brings about a higher E_2 concentration.

This higher E_2 concentration increases E_2 activity.

E_2 concentration increase, which is supposed to increase E_2 activity, should occur over a short period of time. Otherwise, if E_2 activity reaches 1 over a longer time period, meanwhile the F_j drops continue their ascension due to their very low density as compared to the density of the metallic matrix. If the F_j drops are large, they climb to the surface of the metallic matrix at higher rates and consequently the amount of phase 2 diminishes.

The E_2 particles are not evenly distributed in the metallic matrix. Therefore, the case shown by the 1st sequence of Fig. 2 is not what actually happens in industrial practice. Fig. 2 is an ordered geometrical representation in several sequences marked I, II, III and IV.

Although the F_j drops never cease climbing to the surface, the E_2 atoms gather at the phase 1-phase 2 interface, when the ascension rate is not too high, *i.e.* when the F_j drops are small.

The 2nd sequence in Fig. 2 shows the E_2 atom concentration around the interface.

When E_2 activity reaches 1 in an E_2 atom agglomeration, an E_2 nucleus occurs, *i.e.* the unit cell of the E_2 single crystal is formed.

Since the E_2 atoms keep “arriving” from the metallic matrix by diffusion, the attractive forces between the atoms cause the nuclei to grow, *i.e.* they trigger single crystal formation. The 3rd sequence in Fig. 2 illustrates E_2 nuclei formation, the nuclei being symbolized by asterisks. It is obvious that in reality the distances between the E_2 nuclei are not equal, as shown by the 3rd sequence. Moreover, let us not forget that the metallic matrix is multi-component and the chemical elements E_i , ($i = 3, 4, 5, \dots$), are unevenly distributed in solvent E_1 , which results in high E_2 diffusion coefficient gradients in the metallic matrix.

The E_2 nuclei grow in different manners, depending on its crystallization system. For representation simplicity reasons, Fig. 2 chose the hexagonal system as crystallographic system for the element E_2 , a system that only has two types of bonds between the atoms, namely covalent and Van der Waals. A hexagonal system single crystal may be tabular and it may grow as small leaves, *i.e.* small plates. Hence, the attractive forces between the atoms in the small leaves are very strong, *i.e.* of the covalent type. Thus, according to this example, the E_2 single crystals grow mainly in the small leaf plane, while their perpendicular growth on the small leaves is less significant, since the attractive forces between two atoms found in different planes are weak, *i.e.* of the Van der Waals type.

The E_2 nuclei start growing in a plane that follows the outline of the F_j drops and only inside the F_j drops, as the direction and sense of growth are always those that provide the minimum growth energy.

The E_2 nuclei grow in the plane following the outline of the F_j drops, unlike their initial growth, which was free. The E_2 nuclei growth increases F_j particle pressure in the drops, as the free volume of the drops starts to diminish. Thus, the F_j particles start moving towards the outside of the drops. As the F_j particles fail to dissolve in the metallic matrix, they will gather only at the metallic matrix-drop interface.

The E_2 single crystals grow at a considerable rate in the plane that expands. At the same time, few E_2 atoms are attracted by the atoms in the already formed plane, which means that the E_2 crystal also grows perpendicularly on the initial plane, *i.e.* it gets thicker. This is how the initial plane grows, *i.e.* this is how the E_2 single crystal takes shape.

The thickness of the E_2 single crystal depends on the size of the E_2 single crystal in plane. Hence, if the plane expands more, *i.e.* on a larger area of the drop surface, the single crystal is thicker, too.

When the first planes meet, the single crystal stops growing perpendicularly on the main plane. Fig. 3 shows the growth sequences of the first single crystals on the F_j drop surface.

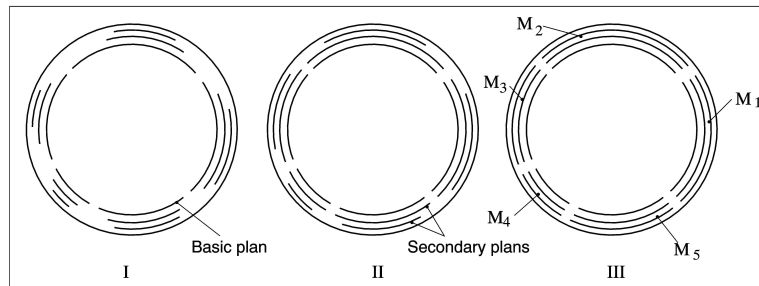


Fig. 3 – Growth sequences of the first layer of single crystals (small leaves or plates). M_1 , M_2 , M_3 , M_4 and M_5 – single crystals; detailed view of the 4th and 5th sequences in Fig. 2.

After all the E_2 atom layers have grown and met, according to the drawing in Fig. 3 (for exemplification purposes, Fig. 3 only shows five E_2 atom layers), the single crystals in the first layer are completed. No new atom layers are formed, since the E_2 single crystals block one another. The single crystal outline is very irregular, which leaves rather large interstices between these single crystals. These interstices help maintain the direct connection between the metallic matrix and phase 2. This is how E_2 particle agglomerations are formed in the vicinity of those single crystal interstices, at the metallic matrix-drop interface, which leads to the formation of new nuclei (5th sequence in Fig. 2). The new nuclei start growing due to the E_2 atoms that keep “arriving” by diffusion from the metallic matrix. As the E_2 nuclei are formed in a random position in relation to the completed single crystals, the E_2 nuclei growth cause

the E_2 single crystals to be displaced, yet not parallel to the outer surface of the F_j drops, but randomly, as shown in the 6th sequence of Fig. 2.

The E_2 nuclei growth phenomenon is repeated as in the sequences marked IV and V.

When the E_2 single crystal leaves its initial position, it creates wide interstices, through which the F_j atoms move towards the outside of the F_j drops and which allow the direct contact between the metallic matrix and phase 2. This is a must for the continuity of the E_2 particle diffusion process from the metallic matrix towards phase 2. Therefore, all the F_j atoms may finally get out of the drops, at the metallic matrix-phase 2 interface.

After the F_j drop has filled with E_2 single crystals and after all the F_j atoms have diffused towards the outside of the drop, a new phase, *i.e.* phase 3, is considered completed. This phase is actually a crystalline body of E_2 single crystals – 7th sequence in Fig. 2.

If the E_2 particles are ions (positive ions, *i.e.* cations), when the E_2 ions approach the F_j drops, they receive electrons from the F_j atoms and they turn into atoms, subsequently forming the E_2 nuclei. Before being attracted by the other E_2 atoms in the growing E_2 single crystal, an E_2 ion always “receives” electrons from the F_j element atoms, turning into an atom.

The F_j particle diffusion phenomenon from the inside to the outside of the drops is continuous during the E_2 single crystal growth process, which means that the electrons needed by the E_2 ions to turn into atoms are continuously available, too.

The F_j particle displacement inside the drops is also thought to occur under the influence of the mechanical equilibrium between the F_j drop and the metallic matrix. When the E_2 nuclei start growing in the drops, the pressure in the drop increases, whereas the pressure in the metallic matrix is constant. The tendency towards mechanical equilibrium between the metallic matrix and the drops takes the form of F_j particle diffusion from the drops towards the metallic matrix. As the chemical element F_j does not dissolve in the metallic matrix, the F_j particles will be distributed around the transforming drop, *i.e.* around the drop that is turning into phase 3. Therefore, the E_2 single crystal growth in the F_j drop is accompanied by the F_j particle diffusion from the drop to the metallic matrix-drop interface or to the metallic matrix-forming phase 3 interface.

Large drops are not filled with E_2 crystals, since they have high ascension rates and, hence, they are removed from the metallic matrix. From this point of view, phases 2 are preferred in industrial practice, due to their high density, which is closer to the density of the metallic matrix. In other words, phases 2 in the liquid state are preferred, since their chemical composition may be easily varied.

Phase 2 is outside the thermodynamic equilibrium, which means that it will always tend to leave the metallic matrix. As the density of the phase 2 drops is very low, the F_j drops will always be removed from the metallic matrix,

regardless of their size.

Phase 3 is, too, outside the thermodynamic equilibrium, which determines its instability and tendency to dissolution in the metallic matrix.

The E_2 atoms in the E_2 single crystals dissolve in the metallic matrix since they originated in this very matrix. Phase 3 dissolves very quickly in the metallic matrix, which means that the metallic matrix should solidify quickly, too, in order to prevent phase 3 from dissolving in the metallic matrix or to allow it to dissolve insignificantly.

If we want phase 3 to dissolve in the metallic matrix with difficulty, the element F_j should be adsorbed to phase 3, since the adsorption forces will prevent the dissolution of phase 3, *i.e.* it will inhibit the phase 3 dissolution process for a relatively long time. This enables us to conclude that the element F_j must meet the second compulsory requirement, *i.e.* to be adsorbed on phase 3.

The element F_j is generally very reactive to some of the elements E_i in the metallic matrix, which finally leads to the F_j - E_i interaction and to the formation of $E_{i_x} F_{j_y}$ chemical compounds that are separated at the surface of the metallic matrix. The F_j particles are thus desorbed from phase 3, and the latter will dissolve in the metallic matrix, thus compromising the inoculation process.

To conclude with, the element F_j should not dissolve in the metallic matrix and it should be adsorbed on phase 3 instead.

If phase 3 dissolution partially occurs during metallic matrix temperature decrease, the E_2 concentration increases in the metallic matrix.

If the entire phase 3 dissolves, the E_2 concentration in the metallic matrix reaches the initial concentration in the metallic matrix, before phase 2 creation.

3. Experiment and Results

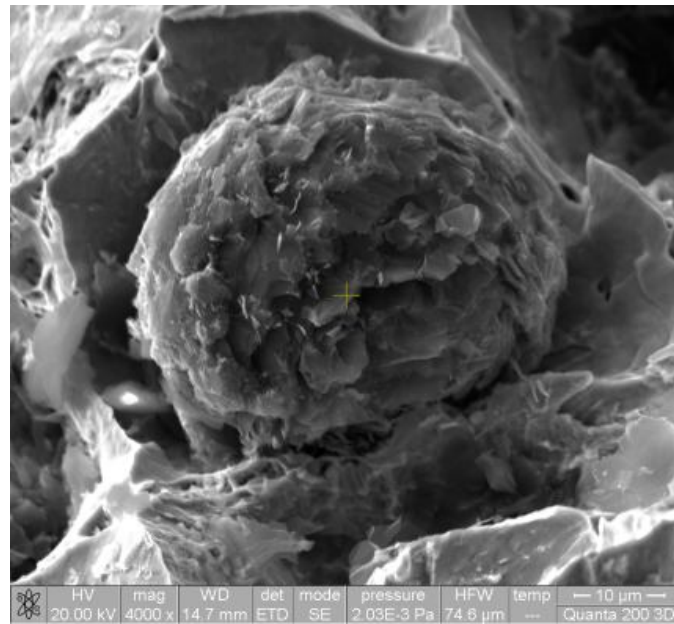
Iron was manufactured in an electric induction furnace with 15 kg capacity.

Liquid iron that was inoculated had the following chemical composition: C = 4.2%; Si = 3%; Mn = 0.8%; P = 0.12%; S = 0.06%; Fe=balance.

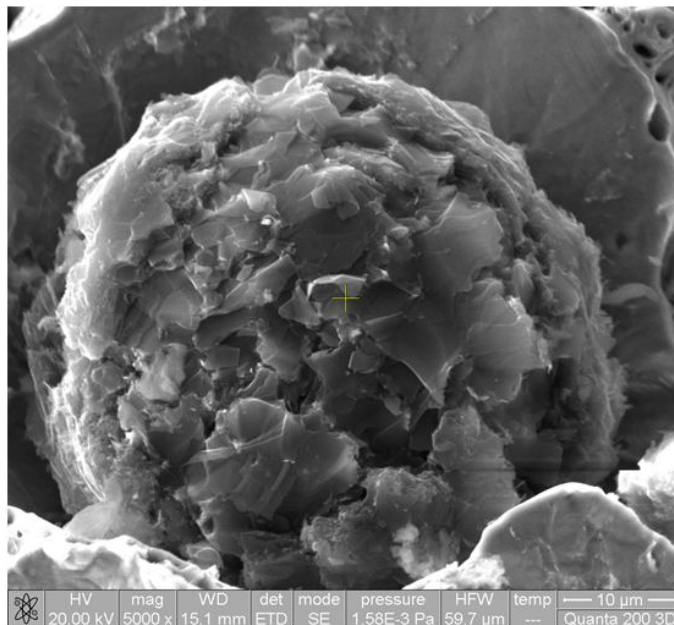
Inoculating agent had the following chemical composition: Mg = 9.5%; Si = 45%; Ca = 1.5%; Fe = balance.

Consumption of inoculating agent was 2%.

In Fig. 4 *a* it is represented an overview of a graphite nodule that was analyzed at an electronic microscope Quanta 200 3-D (Dual Beam – FEI Company – 2007), magnification of 4000 times and in Fig. 4 *b* it is represented a detail of the same graphite nodule.



a



b

Fig. 4 – Image of a graphite nodule, made at an electronic microscope Quanta 200 3D – mag. 4000: *a* – overview image; *b* – detail image.

4. Discussion

Fig. 4 confirms sequence VII from Fig. 2. So, one sees graphite microcrystals as foils of different sizes and having a diverse placing in the space.

5. Conclusion

Explanation of nodular graphite obtaining in liquid iron by the tendency to the chemical equilibrium between two thermodynamic phases (metallic matrix and inoculating agent) is confirmed by experiment and structure analysis with a magnification of 4,000.

REFERENCES

- Cojocaru-Filipiuc V., *Hypotheses on the Production of Metallic Materials Based on the Chemical Equilibrium Tendency – Applications for Cast Iron Inoculation*. Edit. Politehniun, Iași, 2011.
- Cojocaru-Filipiuc V., *Nodulizarea grafitului în fonte – aspect teoretice*. Edit. Politehniun, Iași, 2007.

MECANISMUL OBȚINERII GRAFITULUI NODULAR, PRIN MODIFICARE, PENTRU O FONTĂ TEHNICĂ, CU MODIFICATOR LICHID LA TEMPERATURA DE MODIFICARE

(Rezumat)

Se prezintă schema de modificare a fontei, în cazul în care modificatorul este sub formă de picături în fonta lichidă. La baza schemei, stă legea echilibrului termodinamic ce se stabilește între două faze aflate în contact. Experimentul confirmă umplerea picăturilor de modificador cu monocristale de grafit sub formă de foițe. Experimentul confirmă schema de inoculare. Analiza este realizată la un microscop electronic Quanta 200 3-D, la mărirea de 4000 ori.

BULETINUL INSTITUTULUI POLITEHNIC DIN IAȘI
Publicat de
Universitatea Tehnică „Gheorghe Asachi” din Iași
Tomul LX (LXIV), Fasc. 1-2, 2014
Secția
ȘTIINȚA ȘI INGINERIA MATERIALELOR

BIODEGRADABLE METALLIC MATERIALS APPLICATIONS

BY

FLORIN SĂNDULACHE*, **SERGIU STANCIU**, **NICANOR CIMPOEȘU**
and RAMONA CIMPOEȘU

“Gheorghe Asachi” Technical University of Iași
Faculty of Material Science and Engineering

Received: March 10, 2014

Accepted for publication: March 28, 2014

Abstract: Biodegradable materials represent the opportunity of applying a special class of materials in medical field for temporary materials applications. In this article we present the main applications of the metallic biodegradable materials applied or propose in scientific literature. We present the applications of different systems of materials like Mg-, Fe- and Zn- based alloys with the comparison of the corrosion rates of mentioned systems.

Keywords: biodegradable; metallic materials; degradation rate.

1. Introduction

The development of society and improvement of living standards, the expectation for a better quality of life has been increasing. Scientists have to develop new materials and technologies in order to provide implants with higher clinical performance. In practical clinic applications, some specific clinical problems (such as bone fracture and vessel blockages) need only temporary support for tissue healing process. This temporary sustain can only be provided by an implant made of degradable biomaterials which allow the implant to progressively degrade after fulfilling its biological function.

*Corresponding author: *e-mail*: florinsandulache@yahoo.com

The concept of biodegradation has been known in medical applications for a long time, such as the use of biodegradable polymer sutures. However, implants that degrade, especially those made of metals and alloys, can be considered as a novel concept which actually breaks the established paradigm of “metallic biomaterials must be corrosion-resistant” (Hermawan, 2012).

The definition of biodegradable metals (BMs) had been given as follows: BMs are metals expected to corrode gradually *in vivo*, with an appropriate host response elicited by released corrosion products, then dissolve completely upon fulfilling the mission to assist with tissue healing with no implant residues. Therefore, the major component of BMs should be essential metallic elements that can be metabolized by the human body, and demonstrate appropriate degradation rates and modes in the human body (Zheng *et al.*, 2014).

From the point of view of the materials science, BM can be classified as follows:

A. *Pure metals* (BM-PM)

This category includes the metals mainly composed of one metallic element, with impurity levels lower than the commercial tolerance limits. The corrosion rates of biodegradable metals in this category are mainly driven by the included trace of impurities.

B. *Biodegradable alloys* (BM-BA)

This category encompasses biodegradable metals with various microstructures and one or more alloying elements. Given the concerns for bio-safety of the corrosion products, the alloying elements and their quantities should be controlled without causing adverse pathophysiological and toxicological effects. BM-BA also encompasses biodegradable metallic glasses and biodegradable single crystal metals, which exhibit glassy or single crystal states, respectively, and intend to readily corrode in the human body.



Fig. 1 – Coronary stent made of biodegradable metallic material.

C. Biodegradable metal matrix composites (BM-MC)

This category requires that all components within the composites are biodegradable with the major component being a biodegradable metal. Fundamentally, the bottom line is that the materials are non-toxic to the body.

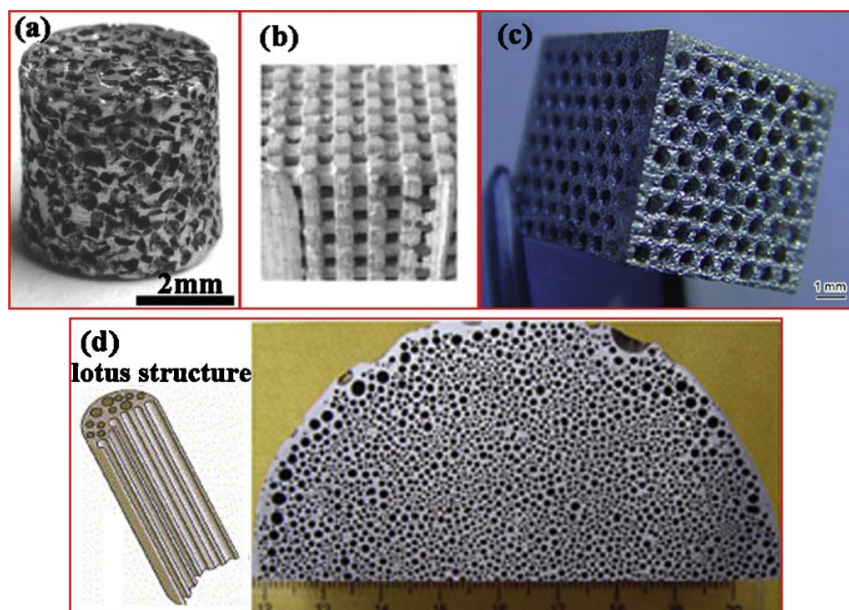


Fig. 2 – *a* – AZ91D scaffold prepared using NaCl as spacer (Witte *et al.*, 2007a, 2007b); *b* – Mg scaffold designed by CAD and the following negative pattern molding (Staiger *et al.*, 2010); *c* – honeycomb-structured magnesium scaffolds fabricated by laser perforation technique (Geng *et al.*, 2009); *d* – lotus-type porous pure magnesium prepared by metal/gas eutectic unidirectional solidification method (Gu *et al.*, 2010).

When metals react with body fluid, they give away electrons and form positive ions. In electrochemistry, the values of standard electrode potential provide a way to compare the relative ease of different metal elements to lose electrons to form ions in solutions. For some metals, they have a much greater tendency to form their ions than hydrogen does; an element is more ready to lose electrons and forms ions, the more negative its standard electrode potential value is. In other words, the more negative the standard electrode potential value is, then the more readily the metal degrades in an aqueous solution.

Fig. 3 illustrates the degradation mechanism of the BM in a physiological environment. Immediately after contacting the body fluid, the BM is oxidized into metal cations following the anodic reaction. The generated electrons are consumed by a cathodic reaction corresponding to the water

reduction for Mg-based BMs and the dissolved oxygen reduction for Fe-based BMs. These reactions occur arbitrarily over the entire surface where a galvanic coupling forms due to different potentials between the metal matrix and intermetallic phase, or grain boundary, as shown in Fig. 2 a. Simultaneously, the organic molecules, such as proteins, amino acids and lipids, will adsorb over the metal surface, thereby influencing the dissolution of BM (Figs. 2 a and 2 b). The $M(OH)_n$ corrosion product layer is expected to form on the metal surface.

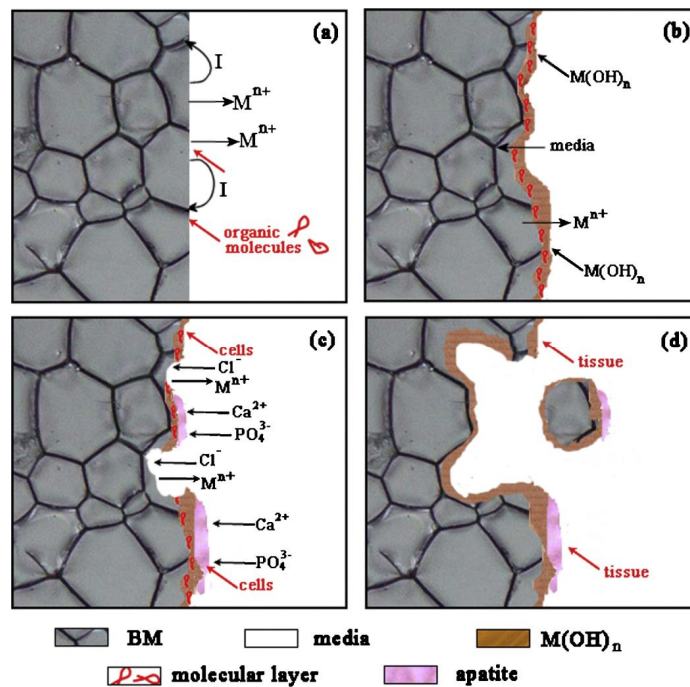


Fig. 3 – Schematic diagram of the biocorrosion at BM/medium interface.

However, the physiological environment is highly aggressive, especially due to the high concentration of chloride ions, which is normally fatal to the metallic hydroxide protective layer. Chloride adsorption causes the breakdown of the $M(OH)_n$ protective layer and leads to pitting corrosion (Fig. 2 c). Generally, the corrosion of Fe-based BMs in pits is self-catalysis since the chloride ions tend to accumulate in pits and the pH of the solutions decreases in aqueous solutions (Song & Shayan, 1998). The corrosion caused no alkalization to Hank's solution (Zhang *et al.*, 2010)[59] whereas the deep undermining of corrosion pits in Mg-based BMs rarely occurs given the fast localized alkalization and the repassivation of the $M(OH)_n$ layer. As the degradation proceeds, calcium phosphate based apatite deposits onto the undissolved $M(OH)_n$ layer due to the localized alkalization and the saturation of calcium and phosphate in the body fluid. Cells are also observed to adhere on

the surface. With progressing implantation time, the adhered cells proliferate to form tissues adjacent to the corrosion product layer. Meanwhile, eroded BM may disintegrate from the whole BM matrix as irregular particles and fall into surrounding media. Such phenomenon is often observed on Mg-based BMs but rarely seen on Fe-based BMs. Depending on the particle size, the fibrous tissue or macrophages might enclose these particle, which may be further degraded until the metallic phase is completely exhausted (Fig. 2 *d*).

Till now, the newly-developed BMs include three main body systems: Mg-based BMs (Manivasagam & Suwas, 2014; Li *et al.*, 2008; Li *et al.*, 2014; Berglund *et al.*, 2012; Gu *et al.*, 2012; Hort *et al.*, 2010; Gu *et al.*, 2010) (pure Mg, Mg–Ca alloys, Mg–Zn alloys, Mg–Sr alloys, Mg–RE alloys, Mg-based bulk metallic glasses (BMGs), etc.), Fe-based BMs (Schinhammer *et al.*, 2010; Schinhammer *et al.*, 2013; Liu & Zheng, 2011; Liu *et al.*, 2011) (pure Fe, Fe–Mn alloys, Fe–W alloys etc.), Zn-based BMs (Jiao *et al.*, 2010; Bowen *et al.*, 2013; Vojtech *et al.*, 2011; Wang *et al.*, 2007) (pure Zn, Zn–Mg alloys and Zn-based bulk metallic glasses) and other BMs (Ca-based (Wang *et al.*, 2011; Li *et al.*, 2010; Cao *et al.*, 2012; Li *et al.*, 2013) and Sr-based BMGs (Zhao *et al.*, 2009; Li *et al.*, 2012; Zhao *et al.*, 2012), etc.). Fig. 4 shows the research status of the three main body BM systems: Mg-based BMs (Li *et al.*, 2008; Gu *et al.*, 2012; Gu *et al.*, 2010; Al-Abdullat *et al.*, 2001; Zartner *et al.*, 2005; Witte *et al.*, 2005; Witte *et al.*, 2006; Erbel *et al.*, 2007; Gu *et al.*, 2009; Zberg *et al.*, 2009; Gu *et al.*, 2011a, 2011b; Ye *et al.*, 2012; Haude *et al.*, 2013; Zhou *et al.*, 2013; Li *et al.*, 2013; Wong *et al.*, 2013; Leung *et al.*, 2013; Zeng *et al.*, 2014; Li *et al.*, 2014; Wang *et al.*, 2014; Han *et al.*, 2014), Fe-based BMs (Liu *et al.*, 2011a, 2011b; Peuster *et al.*, 2001; Peuster *et al.*, 2006; Hermawan *et al.*, 2007; Waksman *et al.*, 2008; Nie *et al.*, 2010; Cheng *et al.*, 2014; Huang *et al.*, 2014), and Zn-based BMs (Bowen *et al.*, 2013; Vojtech *et al.*, 2011; Wang *et al.*, 2007; Jiao *et al.*, 2011; Iva, 2013; Yao *et al.*, 2011). It is quite clear that among these BMs, Mg-based BMs (Manivasagam & Suwas, 2014; Li *et al.*, 2008; Li *et al.*, 2014; Berglund *et al.*, 2012; Gu *et al.*, 2012; Hort *et al.*, 2010; Gu *et al.*, 2010) are the research's vanguard and main force with hundreds of publications on the *in vitro* cytotoxicity, animal testing and clinical trails, Fe-based BMs (Schinhammer *et al.*, 2010; Schinhammer *et al.*, 2013; Liu *et al.*, 2011a; Liu *et al.*, 2011b) are reported in tens of publications on alloy design and several animal testing as potential vascular stent, Zn-based BMs (Jiao *et al.*, 2010; Bowen *et al.*, 2013; Vojtech *et al.*, 2011; Wang *et al.*, 2007) are referred with less than ten publications but seems to be a rising star in the family of biodegradable metals.

Table 1 summarizes the corrosion rates of the Mg-, Fe-, and Zn-based BMs. Considering Mg-based BMs need decreased degradation rate while the Fe-based BMs need enhanced degradation rate, Zn-based BMs are believed to be the next rising stars in the BM family.

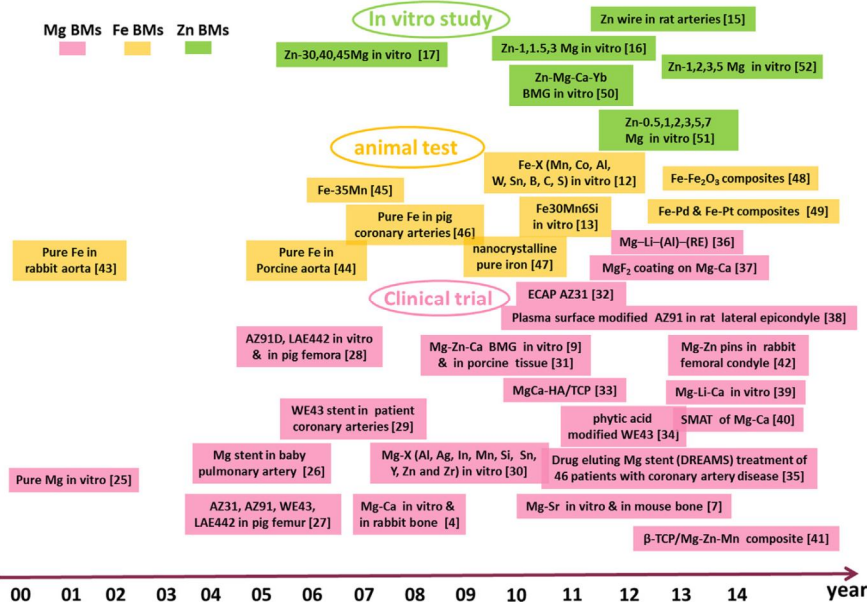


Fig. 4 – Research status of the three BM systems: Mg-based BMs, Fe-based BMs and Zn-based BMs.

Table 1
Comparison of the Corrosion Rates of the Mg-, Fe- and Zn-based BMs

Alloy system	State	In vitro, [mm/year]		In vivo mm/year	References	
		Electro-chemical test	Immersion test			
Mg BMs	Mg	0.20	0.10 ± 0.1		Zhang <i>et al.</i> , 2010	
	Mg-6Zn	Extruded	0.16	0.07 ± 0.02	2.32 ± 0.11	Zhang <i>et al.</i> , 2010
	Mg-1Ca	Cast		12.56	1.27	Li <i>et al.</i> , 2008
	LAE442	Cast	6.9	5.535	0.46 ± 0.11	*
	Mg-10Gd	Cast				Hort <i>et al.</i> , 2010
	Mg-8Y	Cast	2.17 ± 0.23	1.25 ± 0.2	0.39 ± 0.1	Peng <i>et al.</i> , 2010
	Mg-0.8Ca	Extruded				Thomann <i>et al.</i> , 2009
Mg-2Sr	Rolled	0.87 ± 0.08	0.37 ± 0.05	1.01 ± 0.07	Gu <i>et al.</i> , 2012	
Fe BMs	Fe	Cast	0.105	0.012		Liu <i>et al.</i> , 2011a
	Fe-2W	SPS	0.075	0.026		Cheng <i>et al.</i> , 2013
	Fe-0.5CNT	SPS	0.099	0.048		Cheng <i>et al.</i> , 2013
	Fe-Mn	Cast	0.105	0.0018		Liu & Zheng, 2011a
	Fe-W	Cast	0.151	0.016		Liu & Zheng, 2011a
Zn BMs	Zn	Cast		0.08	0.02	Vojtech <i>et al.</i> , 2011
	Zn-1Mg	Cast		0.09		Vojtech <i>et al.</i> , 2011

* Witte *et al.*, 2006; Erbel *et al.*, 2007; Gu *et al.*, 2009; Zberg & Uggowitzer, 2009; Gu *et al.*, 2011a; Gu *et al.*, 2011b; Ye *et al.*, 2012; Haude *et al.*, 2013; Zhou *et al.*, 2013; Li *et al.*, 2013; Wong *et al.*, 2013; Zeng *et al.*, 2014; Li *et al.*, 2014; Wang *et al.*, 2014; Han *et al.*, 2014; Peuster *et al.*, 2001; Peuster *et al.*, 2006; Hermawan *et al.*, 2007; Waksman *et al.*, 2008; Nie *et al.*, 2010; Cheng *et al.*, 2014; Huang *et al.*, 2014; Jiao *et al.*, 2011; Iva, 2013; Yao *et al.*, 2011; Zhang *et al.*, 2010; Witte *et al.*, 2010.

2. Medical Applications of Biodegradable Metallic Materials

Broadly, biomedical implants encompass a range of medical solutions for various bodily disorders and include: (i) cardiovascular implantable devices like stents, vascular grafts, heart valves, defibrillators, pace- makers, etc. (ii) neural devices like neuronal implants and prostheses for central nervous system (CNS), peripheral nervous system (PNS), co- chlear and retinal applications (iii) orthopedic prostheses like bone grafts, bone plates, fins and fusion devices; orthopedic fixation devices such as interference screws in the ankle, knee, and hand areas, rods and pins for fracture fixation, screws and plates for craniomaxillo facial repair; bone tissue engineering scaffolds for fractures and general implants which forms the scope of the current article (Fig. 5).

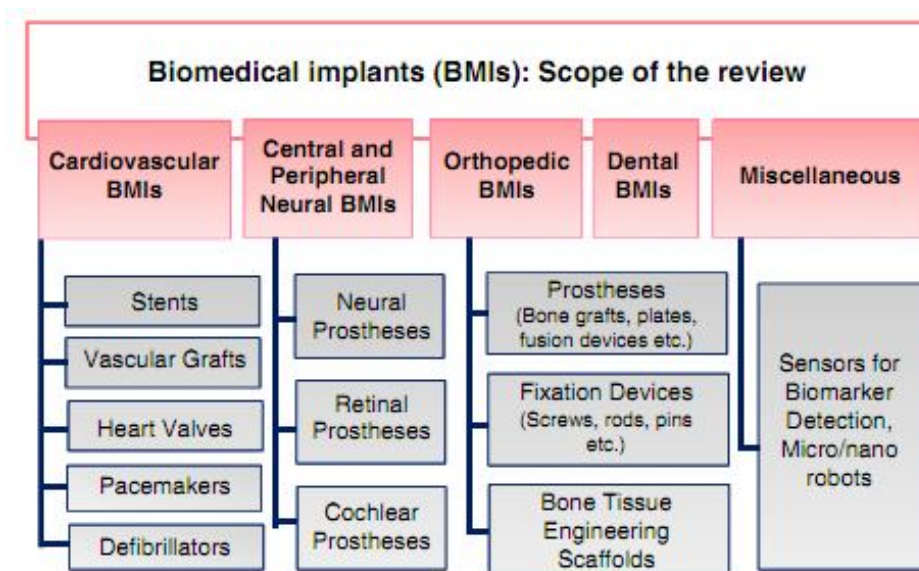


Fig. 5 – Biomedical implants (BMIs): scope of the review.

2.1. Stents

Stents have contributed greatly to the development of interventional catheterization for CHD. From the old rigid Palmaz stent to covered and valve stents, technological evolution has further extended their clinical applications. The interventionists have to deal with the number and different properties of available endo-prosthesis to choose the appropriate stent for each case. Results are good and stenting has become a validated alternative to surgery in many lesions.

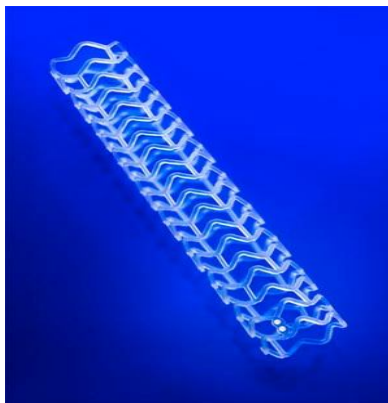


Fig. 6 – Coronary stent.

Miniaturization of delivery systems would facilitate implantation in tortuous and small vessels. The inability of stents to follow natural vessel growth remains an important limitation to their use in growing children. Biodegradable stents with sufficient radial strength but respecting natural vessel growth may further extend the use in infants and neonates.

2.2. Biodegradable Orthopedic Devices

Procedures can still be lengthy and complex but may be facilitated in many cases by fusion imaging and periprocedural three-dimensional guidance. Large sheaths required for stent deployment limit use and increase the risk of vessel access complications.

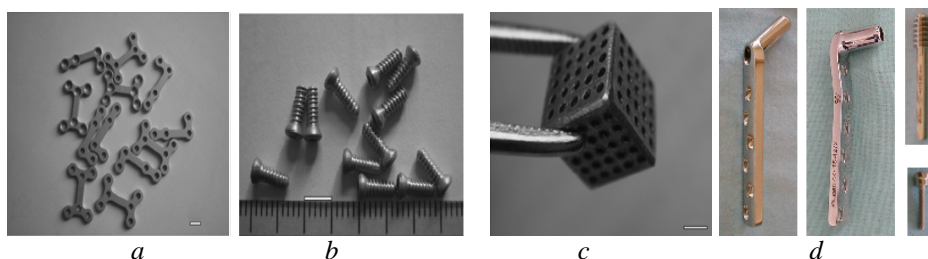


Fig. 7 – Biodegradable orthopedic devices prepared from Mg and its alloys: *a* – bone plates; *b* – screws for orthopedic fixation; *c* – a porous scaffold for bone void filling. Scale bar = 10 mm. (Karagkiozaki *et al.*, 2012); *d* – Orthopedic screws and rods (www.valdomedica.ro...).

3. Conclusions

Worldwide, bio-medical implants gather a range of medical solutions for various bodily disorders which include cardiovascular implantable devices

like stents, vascular grafts, heart valves, defibrillators, pace- makers, neural devices like neuronal implants and prostheses for central nervous system (CNS), peripheral nervous system (PNS), cochlear and retinal applications, orthopedic prostheses like bone grafts, bone plates, fins and fusion devices; orthopedic fixation devices such as interference screws in the ankle, knee, and hand areas, rods and pins for fracture fixation, screws and plates for cranio-maxillo facial repair; bone tissue engineering scaffolds for fractures and dental implants which forms the scope of the current article.

REFERENCES

- Hermawan H., *Biodegradable Metals: State of the Art*. Biodegradable Metals, Springer, 2012, 13-22.
- Zheng Y.F., Gu X.N., Witte F., *Mat. Sci. Engng.*, **R 77**, 1-34 (2014).
- Manivasagam G., Suwas S., *Mater. Sci. Technol.*, **30**, London, 515-520 (2014).
- Li Z.J., Gu X.N., Lou S.Q., Zheng Y.F., *Biomaterials*, **29**, 1329-1344 (2008).
- H. Li, Q.M. Peng, X.J. Li, K. Li, Z.S. Han, D.Q. Fang, *Mater. Des.* 58 (2014)43–51.
- Berglund I.S., Brar H.S., Dolgova N., Acharya A.P., Keselowsky B.G., Sarntinoranont M., Manuel M.V., *J. Biomed. Mater. Res.*, **B, 100B**, 1524-1534 (2012).
- Gu X.N., Xie X.H., Li N., Zheng Y.F., Qin L., *Acta Biomater.*, **8**, 2360-2374 (2012).
- Hort N., Huang Y., Fechner D., Stormer M., Blawert C., Witte F., Vogt C., Drucker H., Willumeit R., Kainer K.U., Feyerabend F., *Acta Biomater.*, **6**, 1714-1725 (2010).
- Gu X.N., Zheng Y.F., Zhong S.P., Xi T.F., Wang J.Q., Wang W.H., *Biomaterials*, **31**, 1093-1103(2010).
- Schinhammer M., Hanzi A.C., Loffler J.F., Uggowitzer P.J., *Acta Biomater.*, **6**, 1705-1713 (2010).
- Schinhammer M., Gerber I., Hanzi A.C., Uggowitzer P.J., *Mat. Sci. Eng. C – Mater.*, **33**, 782-789 (2013).
- Liu B., Zheng Y.F., *Acta Biomater.*, **7**, 1407-1420 (2011a).
- Liu B., Zheng Y.F., Ruan L.Q., *Mater. Lett.*, **65**, 540-543 (2011b).
- Jiao W., Zhao K., Xi X.K., Zhao D.Q., Pan M.X., Wang W.H., *J. Non- Cryst. Solids*, **356**, 1867-1870 (2010).
- Bowen P.K., Drelich J., Goldman J., *Adv. Mater.*, **25**, 2577-2582 (2013).
- Vojtech D., Kubasek J., Serak J., Novak P., *Acta Biomater.*, **7**, 3515-3522 (2011).
- Wang X., Lu H.M., Li X.L., Li L., Zhenh Y.F., Nonferr T., *Metal. Soc.*, **17**, S122-S125 (2007).
- Wang Y.B., Xie X.H., Li H.F., Wang X.L., Zhao M.Z., Zhang E.W., Bai Y.J., Zheng Y.F., Qin L., *Acta Biomater.*, **7**, 3196-3208 (2011).
- Li H.F., Wang Y.B., Cheng Y., Zheng Y.F., *Mater. Lett.*, **64**, 1462-1464 (2010).
- Cao J.D., Kirkland N.T., Laws K.J., Birbilis N., Ferry M., *Acta Biomater.*, **8**, 2375-2383 (2012).
- Li H.F., Xie X.H., Zhao K., Wang Y.B., Zheng Y.F., Wang W.H., Qin L., *Acta Biomater.*, **9**, 8561-8573 (2013).

- Zhao K., Li J.F., Zhao D.Q., Pan M.X., Wang W.H., *Scr. Mater.*, **61**, 1091-1094 (2009).
- Li H.F., Zhao K., Wang Y.B., Zheng Y.F., Wang W.H., *J. Biomed. Mater. Res.*, **B**, *100B*, 368-377 (2012).
- Zhao K., Jiao W., Ma J., Gao X.Q., Wang W.H., *J. Mater. Res.*, **27**, 2593-2600 (2012).
- Al-Abdullat Y., Tsutsumi S., Nakajima N., Ohta M., Kuwahara H., Ikeuchi K., *Mater. Trans.*, **42**, 1777-1780 (2001).
- Zartner P., Cesnjevar R., Singer H., Weyand M., *Catheter. Cardiovasc. Interv.*, **66**, 590-594 (2005).
- Witte F., Kaese V., Haferkamp H., Switzer E., Meyer-Lindenberg A., Wirth C.J., Windhagen H., *Biomaterials*, **26**, 3557-3563 (2005).
- Witte F., Fischer J., Nellesen J., Crostack H.A., Kaese V., Pisch A., Beckmann F., Windhagen H., *Biomaterials*, **27**, 1013-1018 (2006).
- Erbel R., Di Mario C., Bartunek J., Bonnier J., de Bruyne B., Eberli F.R., Erne P., Haude M., Heublein B., Horrigan M., Ilesley C., Bose D., Koolen J., Luscher T.F., Weissman N., Waksman R., *Lancet*, **369**, 1869-1875 (2007).
- Gu X.N., Zheng Y.F., Cheng Y., Zhong S.P., Xi T.F., *Biomaterials*, **30**, 484-498 (2009).
- Zberg B., Uggowitzer P.J., Loffler J.F., *Nat. Mater.*, **8**, 887-891 (2009).
- Gu X.N., Li N., Zheng Y.F., Kang F., Wang J.T., Ruan L.Q., *Mater. Sci. Eng. B – Adv.*, **176** 1802-1806 (2011a).
- Gu X.N., Wang X., Li N., Li L., Zheng Y.F., Miao X.G., *J. Biomed. Mater. Res.*, **B**, *99B*, 127-134 (2011b).
- Ye C.H., Zheng Y.F., Wang S.Q., Xi T.F., Li Y.D., *Appl. Surf. Sci.*, **258**, 3420-3427 (2012).
- Haude M., Erbel R., Erne P., Verheye S., Degen H., Bose D., Vermeersch P., Wijnbergen I., Weissman N., Prati F., Waksman R., Koolen J., *Lancet*, **381**, 836-844 (2013).
- Zhou W.R., Zheng Y.F., Leeftang M.A., Zhou J., *Acta Biomater.*, **9**, 8488-8498 (2013).
- Li N., Li Y.D., Wang Y.B., Li M., Cheng Y., Wu Y.H., Zheng Y.F., *Surf. Interface Anal.*, **45**, 1217-1222 (2013).
- Wong H.M., Zhao Y., Tam V., Wu S.L., Chu P.K., Zheng Y.F., To M.K.T., Leung F.K.L., Luk K.D.K., Cheung K.M.C., Yeung K.W.K., *Biomaterials*, **34**, 9863-9876 (2013).
- Zeng R.C., Sun L., Zheng Y.F., Cui H.Z., Han E.H., *Corros. Sci.*, **79**, 69-82 (2014).
- Li N., Li Y.D., Li Y.X., Wu Y.H., Zheng Y.F., Han Y., *Mat. Sci. Eng. C – Mater.*, **35**, 314-321 (2014).
- Wang X., Zhang P., Dong L., Ma X., Li J., Zheng Y., *Mater. Des.*, **54**, 995-1001 (2014).
- Han P., Tan M.Y., Zhang S.X., Ji W.P., Li J.N., Zhang X.N., Zhao C.L., Zheng Y.F., Chai Y.M., *Int. J. Mol. Sci.*, **15**, 2959-2970 (2014).
- Peuster M., Wohlsein P., Bruggmann M., Ehlerding M., Seidler K., Fink C., Brauer H., Fischer A., Hausdorf G., *Heart*, **86**, 563-569 (2001).
- Peuster M., Hesse C., Schloo T., Fink C., Beerbaum P., von Schnakenburg C., *Biomaterials*, **27**, 4955-4962 (2006).
- Hermawan H., Dube D., Mantovani D., *Adv. Mater. Res.*, *Switz.*, **15-17**, 107-112 (2007).
- Waksman R., Pakala R., Baffour R., Seabron R., Hellinga D., Tio F.O., *J. Interv. Cardiol.*, **21**, 15-20 (2008).

- Nie F.L., Zheng Y.F., Wei S.C., Hu C., Yang G., *Biomed. Mater.*, **5** (2010).
- Cheng J., Huang T., Zheng Y.F., *J. Biomed. Mater. Res.*, **A**, *102*, 2277-2287 (2014).
- Huang T., Cheng J., Zheng Y.F., *Mat. Sci. Eng. C – Mater.*, **35**, 43-53 (2014).
- Jiao W., Li H.F., Zhao K., Bai H.Y., Wang Y.B., Zheng Y.F., Wang W.H., *J. Non-Cryst. Solids*, **357**, 3830-3840 (2011).
- Iva Pospíšilová D.V., Brno, Czech Republic, EU, 2013.
- Yao C.Z., Wang Z.C., Tay S.L., Zhu T.P., Gao W., *J. Alloy Compd.*, **602** (2011).
- Zhang S.X., Zhang X.N., Zhao C.L., Li J.A., Song Y., Xie C.Y., Tao H.R., Zhang Y., He Y.H., Jiang Y., Bian Y.J., *Acta Biomater.*, **6**, 626-640 (2010).
- Witte F., Fischer J., Nellesen J., Vogt C., Vogt J., Donath T., Beckmann F., *Acta Biomater.*, **6**, 1792-1799 (2010).
- Peng Q.M., Huang Y.D., Zhou L., Hort N., Kainer K.U., *Biomaterials*, **31**, 398-403 (2010).
- Thomann M., Krause C., Bormann D., von der Hoh N., Windhagen H., Meyer-Lindenberg H., *Materialwiss Werkst*, **40**, 82-87 (2009).
- Cheng J., Zheng Y.F., *J. Biomed. Mater. Res.*, **B**, *101B*, 485-497 (2013).
- Song G., Shayan A., *Corrosion of Steel in Concrete: Causes, Detection and Prediction, A state-of-the-Art Review*. Review Report 4, ARRB Transport Research Ltd., Victoria, Vermont, 1998.
- Zhang E., Chen H., Shen F., *J. of Mater. Sci.: Mater. in Medicine*, **21**, 2151-2163 (2010).
- Witte F., Ulrich H., Palm C., Willbold E., *J. of Biomedical Mater. Res., Part A*, **81A**, 757-765 (2007a).
- Witte F., Ulrich H., Rudert M., Willbold E., *J. of Biomedical Mater. Res., Part A*, **81A**, 748-756 (2007b).
- Staiger M.P., Kolbeinsson I., Kirkland N.T., Nguyen T., Dias G., Woodfield T.B.F., *Materials Letters*, **64**, 2572-2574 (2010).
- Geng F., Tan L., Zhang B., Wu C., He Y., Yang J., Yang K., *J. of Mater. Sci. & Technol.*, **25**, 123-129 (2009).
- Gu X.N., Zhou W.R., Zheng Y.F., Liu Y., Li Y.X., *Mater. Lett.*, **64**, 1871-1874 (2010).
- Karagkiozaki V., Karagiannidis P.G., Kalfagiannis N., Kavatzikidou P., Patsalas P., Georgiu D., Logothetidis S., *Novel Nanostructured Biomaterials: Implications for Coronary Stent Thrombosis*. *Intenat. J. Nanomedicine*, **7**, 6063-6076 (2012).
- * * www.valdomedica.ro/ortopedie_traumatologie.html

APLICAȚII ALE MATERIALELOR METALICE BIODEGRADABILE

(Rezumat)

Materialele biodegradabile reprezintă o oportunitate de aplicare a unei clase speciale de materiale din domeniul medical dedicate aplicațiilor cu materiale utilizabile temporar. În acest articol prezentăm principalele aplicații ale materialelor metalice biodegradabile implementate sau propuse în literatura de specialitate. Sunt prezentate aplicații ale unor sisteme diferite de material cum ar fi cele metalice pe bază de Mg, Fe sau Zn și o comparație a vitezei de degradare a acestora.

BULETINUL INSTITUTULUI POLITEHNIC DIN IAȘI
Publicat de
Universitatea Tehnică „Gheorghe Asachi” din Iași
Tomul LX (LXIV), Fasc. 1-2, 2014
Secția
ȘTIINȚA ȘI INGINERIA MATERIALELOR

INNOVATION IN KNOWLEDGE BASED SOCIETY PLASTICS WELDING TECHNOLOGY

BY

MARIA-LUCIANA ATOMEI*

“Gheorghe Asachi” Technical University of Iași
Faculty of Material Science and Engineering

Received: March 10, 2014

Accepted for publication: March 28, 2014

Abstract: A knowledge society generates, processes, shares and makes available to all members of the society knowledge that may be used to improve the human condition.

Ultrasonic assembly is a heat-related process, that can significantly increase production and lower assembly costs, used more and more in automotive design of plastic parts, offering flexibility and versatility not found in many other assembly processes.

This paper presents the effect and methods of the process of welding process in automotive companies in a knowledge based society. Laser welding of plastics is becoming increasingly widespread as it provides many benefits. The study presents welding methods for various products made from composite materials from the large domain of technological and mechanical parameters of the welding process.

Keywords: innovation; information society; knowledge; e-society; welding; technology; plastic welding; composite materials.

1. Introduction

Today, knowledge production systems cover a wide range of entities: universities, laboratories, research centers, government, industry and the private

**e-mail:* luciana_atomei@yahoo.com

sector. These systems have undergone profound transformations to become the main drivers of growth in a globalized world. This has made major changes in the landscape of higher education, particularly in the university sector.

Consequently, all countries worldwide are facing increased demand for their research capacity building and knowledge production. This demand is increasing worldwide, it differs from country to country due to the particularities of contexts given their political, socio-economic and cultural. Thus, each nation according to their own capacity to respond, created and given a new system of national importance knowledge oriented institutions.

It often requires efforts to renew higher education systems and structures for each country to have its place in knowledge-based societies that are both competitive and volatile. In turn, strengthening research and higher education multiplies pressures on funding, content and structure of knowledge systems.

As a critical aspect of ultrasonic welding, the configuration of two mating surfaces it should be considered when the parts to be welded are still in the concept phase, selection of the features being determined by client requirements, type of plastic, molding capabilities and appearance.

To be competitive, innovation is needed - especially in the competitive world of technology. Innovation areas leads to converting research results into innovative products and services.

An economy based on innovation has an advantage competitive, consisting in producing innovative products and services. It means ultimately productivity, but is determined by a range of factors - the quality of the business environment, stimulate investment, innovation capacity and the level of competition.

Company information is based on present society where people depend on a knowledge society and also contains large organizations and corporations. Such knowledge-based organization is an important factor for the group, smart and contemporary belonging both by scientific research and by strategic activity. It is therefore a combination of knowledge and concept organization, defining a solid construction collectively intelligent, efficient and competent.

The organization operates consistent with knowledge and information society is mainly determined by innovation, learning and partnership interactivity. The first mention of the concept of knowledge organization appeared somewhere in the years 1984-1988 and since then until now has undergone many stages of development. In 1984, Huber questioned the need to create an organizational model for organizations especially post - Industrial later, this idea is also found in other operational approaches that propose solutions.

Holsapple and Whinston (1987), promoters of computer technology provides a definition of knowledge-based organization, "a community of

workers with job design, interconnected by a computerized infrastructure". These authors argue advanced IT support organization and applications of artificial intelligence. From the management point of view, in 1988, Drucker is a valid organizational model for the XXI century, with the main features - without many intermediate levels hierarchical leadership, coordination employees by standards, regulations and internal rules of the organization team consists mainly of professionals.

After the year 1955 and the first results of relevant importance in the operation and development of knowledge-based organization, visions time generating new names like "organization centered on memory" (Le Moigne, 1990), "intelligent organization" (Hendriks, 1998).

Case study is made in a department of design and development from Timisoara (Hella) and offers informations about actual methods applied in design of plastic parts – guidelines created for the designers, with basic requirements and compatibility of materials in applying ultrasonic welding. This paper presents main datas of ultrasonic welding process with the design considerations in choice of row materials, the impact and the advantages of using this process in design of plastic parts.

Study is offering up-to-date informations about using ultrasonic welding and what its necessary for a good component design from a highly rated company from the market, informations that can provide us future actions and corrections needed to improve performance in a design and development department.

Basic principles for laser transmission welding of plastics – *Principle of laser transmission welding*

For laser transmission welding of plastics generally a laser absorbing and a laser transmitting material will be welded together. During transmission welding two thermoplastic materials with different absorption properties due to different types or concentrations of fillers are welded at the lan joint (Fig. 1).



Fig. 1 – Lens welded on the housing – automotive lamp.

The plastic parts, which are to be joined, lie on top of each other and the laser beam is focused through the plastic transparent for the laser wave length onto the absorbing formed component through which it melts on the surface.

The transparent partner is also plasticized through thermal conduction which results in the bonding of the materials. In order to ensure the necessary contact of the two joining partners for the thermal conduction process during welding it is necessary to apply pressure by using a clamping device adapted to the component part. The strengths of the weld beam are similar to the one of the full material and reach therefore almost welding factor 1.

2. Process Variants of Transmission Welding of Plastics by Laser

The different kind of process methods of laser transmission welding are structured by their kind of energy insertion: contour welding, simultaneous welding, quasi-simultaneous welding and hybrid welding. All variants show their specific advantages and disadvantages. Which variant or which kind of energy insertion is practical depends on the application and welding parts.

In contrast to the ultrasonic welding, laser welding is easy and flexible, because each curved plastic welding can be programmed. Surface quality material remains unchanged, is a rapid, repetitive, environmentally friendly and requires no bonding agent toxic, as if adhesive labels. Welding can withstand heavy mechanical stress. The heat applied is minimal. This is important when near the weld are sensitive electronic components.

Hybrid welding is a advancement of the contour welding process. In this welding method a second energy source emitting polychromatic light is used additional to the laser beam. According to its bigger focus this polychromatic infrared radiation (halogen emitter with parabolic reflector) heats the welding parts in the joining zone slower and also reaches a slower cooling. So it is possible to reduce or to avoid residual stress in the joining zone and to reach an optimal joining .

With the use of halogen emitter it is also possible to reach a better weld ability of small gaps between the polymers.

3. Material Compatibility

It is not possible to weld every combination of polymers. Here the melting and softening point should be attended. The two polymers, which are to be joined, must be coordinated to each other. It is principally possible to weld thermoplastic materials and numerous thermoplastic elastomers.

The prerequisite for a safe bonding is a minimum chemical compatibility of the two materials. As stated already one of the two joining partners must be designed transparent for wave lengths in the range of 820nm – 980nm, the other material absorbent for this wavelength (*e.g.* carbon pigmentation).

3.1. Accessibility for the Laser Beam

In order to enable an even illumination of the welding contour it must be possible for the laser beam to penetrate right through to the connecting surface without being obstructed. It is to be taken into account that the contour of the laser beam at the first approach has the form of a cone.

Objects located between the joining point and the source of the laser beam must not lie in the optical path of the laser as this will otherwise produce shadowing effects. This problem of shadowing the laser beam is pictured in Fig. 1.

Beside of inapplicable geometries of the welding parts in the most cases the reasons of such a shadowing are wrong positioned hard stops and clamping cylinders at the jig. A specialist of LPKF Laser & Electronics AG, Plastics Welding Division should be involved in the product production process as soon as possible in order for an exact statement to be made regarding the beam diameter and impact angle on the connecting surface.

3.2. Accessibility for the Clamping Roller

In order to enable the necessary permanent pressure on the welding parts an always accessible welding contour on the laser transparent polymer has to be guaranteed. Thereby a continuous contact between the clamping roller and the welding part has to be attended. In best cases the welding part should be a free-form with big radiuses, but by using additional clamping devices on the jig also steps and flanges can be realized.

3.3. Material Thickness

To get a capable welding with good strengths the material thickness is a not marginal parameter. On the one side the laser transparent material has to be thin enough to avoid power loss and mistakes in the weld seam according to the transmission properties. On the other side the material has to be strong enough to transmit the necessary pressure applied through the clamping roller and additional clamping devices (buckling resistance in case of long, thin walls).

Normal values here range between 0.8 mm and 3 mm, depending on the material. However, it is perfectly possible to achieve higher or lower values with individual material combinations.

3.4. Melt Travel

In the majority of applications a welding web on the absorbing polymer will be melted down during the welding process. Therefore the laser transparent

part will be set down to the laser absorbing part upon the pressure of the welding process. According to the thermal conduction both polymers will be melted and joined adhesively. Thereby the melt travel depends on the requirements of the parts, the tolerances and the used material. Typically a melt travel of 0.2,...,0.5 mm should be sufficient.

4. Laser Welding of Plastics – Case Study in Automotive Company – Supplier of Headlamps, Rearlamps, Working Lamps

In the commercial vehicle segment, automotive companies supply products for both series production and vehicle-specific new developments. Customers has benefits from in-depth technical expertise and experience in large-scale automotive manufacturing applications. Depending on the task at hand, customers can choose between halogen, xenon, and LED technology for the lighting system, and can also select from a wide range of electrical and electronic products.

Welding : Substance-to-substance bonds are producing a connection on molecular level by interaction between molecules (*e.g.* van der Waals-forces, secondary valence forces). They demand a very close contact of surfaces. Therefore at least one partner has to be in liquid form. In Welding processes this is achieved by melting the parts. The principal sequence is:

- a) melting the contact surfaces (in contact or bringing them into contact afterwards);
 - b) letting them cool down under pressure.
- Resulting joints are:
- strong;
 - tight;
 - durable;
 - free of relative movements (*i.e.* low noise);
 - non detachable.

Prerequisite on material side is their (molecularly) compatibility. Provided this welding of different polymers is well possible (so-called “mixed material welds”).

- During a welding process normally a movement between the parts is performed.
- Due to this melt is displaced perpendicularly to the joining direction, forming the weld bead.

Contrary to metal-welding the polymer melt is highly viscous and therefore flows luminary. There is no visible intermixing of materials, welded parts still are clearly distinguishable.

There are various models for the explanation of adhesion. None of this alone suffices to fully describe adhesion. Only with all them together the connection between two materials can be approached.

- Mechanical Adhesion (*not relevant for welding*)
- Polarization Theory (electrical interactions of molecular dipoles)
- Wetting and Interface Tension
- Diffusion Theory, Creep Modell
- Molecular stretching and Relaxation
- Chemical bonds (*not relevant for welding*)

1. Placing the housing(s) in the lower tool
2. Placing the lens(es) onto the housing(s)
3. Starting of machine
4. Machine closes and brings the upper tool to the lens(es)
5. Vacuum is activated and lens(es) are sucked into the upper tool
6. After “Suction time” the machine moves back
7. The hot tool (axis 3) is moved in working position
8. Upper and lower tool (axis 1 and 2) are moved towards the hot tool
9. Parts are molten down by contact to the hot tool under pressure
10. Heat energy is brought into the parts without pressure
11. Upper and lower tool (axis 1 and 2) are moved up-/downwards
12. The hot tool (axis 3) is moved back into parking position
13. Upper and lower tool (axis 1 and 2) move together, bring parts in contact and apply the joining force, the welding joint is formed
14. Joining time elapses, parts cool down
15. Vacuum is turned off
16. After joining time has elapsed the machine opens
17. The process ends (door opens, welded parts are taken out)

Tool temperature:

- Tool temperature shall be between
 - 400°C and 430°C for PMMA (lenses)
 - 420°C and 480°C for ABS (housings)
 - 460°C and 480°C for PC+ABS (housings)
- At the lower limit stringing may occur.
- At the upper limit stress cracks due to monomers and damage of metallization may occur.

Heating time:

- The time in which the necessary heat energy is brought into the welding faces.
- Usual times are around 5 to 7 seconds, 15 to 20 seconds for Delta-welding.

Heating time can be different for housing and lens dependent on materials and geometries.

Change-over time:

- The time between taking off the tools and contact of the parts.
- The change-over time shows mayor influence in the welding result.

- It has to be kept as short as possible because the welding areas are cooling down during this period. Change-over time should not be longer than 3 seconds.
- The change-over time depends on the distances which the axes have to be moved and on the inertias of machine and jigs that have to be accelerated and decelerated.

Joining time:

- The time during which the parts are pressed against each other and cool down.
- The Joining time should be approx. 2 seconds longer than the heating time (for high temperature welding). Usual Joining times are around 7-10 seconds.

Joining force:

- The force which is applied to press the parts against each other during joining.
- The joining force results from the size of the welding area and the necessary pressure of **0.7 to 1.0 N/mm²**. Typical Joining forces are around 7 to 10kN (larger welding areas demand higher forces).
- At too high forces the welding rib may be pressed through the molten material. Such welds show nearly no strength (“Cold welds”). This also results in high joining paths.
- Too low forces result in leaky welds. Sometimes defects can also be seen through the lens. This also results in low joining paths.

Joining velocity:

- The speed at which the molten surfaces are pressed into each other.
- This also influences the weld quality.

Melt-down:

- The melt-down denominates the distance that is molten from the welding surfaces of housing and lens. Usual values are approx. 0.5 to 1mm.
- The melt-down depends on the dimensional quality of the parts. Sink marks, protruding ejector pins etc. determine the melt-down value and influence the evenness of appearance of the weld bead.
- It is important to ensure a sufficient melt-down along the whole weld line. Areas with no melt-down won't be joined properly and will be leaky.

Joining path:

- The distance that parts go from contact of molten surfaces to final position.

Remark: To ensure sufficient melt-down along the whole weld line a welding add-on has to be considered in design. From the virtual surface that represents the final interface of parts after welding (“B1” in drawings), the welding areas of both parts have to be elevated to cover melt-down and joining path. This additional melt-down usually is 1mm on each part.

Take up force:

- The force which is applied when closing the machine to take up the lens from the housing.
- This force should be set as low as possible because parts may break when contours aren't well matched. Typical take up forces are between 1 to 10kN.

Suction time:

- The suction time starts when the upper tool has moved to the lens (take up force is reached). After this time the machine moves back.
- The suction time is necessary to ensure a stable formation of vacuum and good grip of the upper tool.

In spite of keeping the same base layout, fixtures were constantly refined. Some keywords:

- **Lower Tool:**

- previously: steel, today: aluminum;
- incorporation of screw and parts verification;
- pneumatic clamping.

- **Upper Tool:**

- vacuum holding with suction by round cord seal;
- previously: steel, today: aluminum;
- upper tool displacement;
- hard coating to prevent damages and contamination.

- **Hot Tool:**

- previously: Steel, today: Cu-Si-Al or "Moldmax";
- thermal expansion of material is considered in tool design;
- hard facing of contact areas/chemical nickel plating to cope with wear;
- close to contour placing of cartridge heaters (again possible with steel)
 $\Delta T \leq 10K$.

5. Conclusions

Lately ultrasonic welding has experienced a great development, mainly due to the close relationship he has with electronics, field recognized as having the greatest growth in the last 40 years. Application of ultrasonic welding in sensitive areas such as electronics was directed by the advantages which it presents. Most often mentioned advantages are related to welding relatively low temperature compared to fusion welding, heating that occurs strictly local, and the possibility of making the joints size from millimeter values to values of centimeters.

Ultrasonic welding is applied at present in a relatively large number of other leading industrial areas. Characterized by high welding speed and mechanical characteristics, tightness and very good electrical bonding process

by ultrasonic welding takes on ever new uses both conventional situations (from household goods to industrial products top) and in unconventional situations.

This theme aims to conduct a study on how to develop the equipment for ultrasonic welding of metallic materials Disimination, and a foray into tehnoilogic ultrasonic welding technology specific mechanisms imposed by the interaction between ultrasound and dissimilar metallic materials undergo the process of joining.

Effectuate documentary research showed absolutely unconventional applications of ultrasound, which, besides thermal sources welding processes are useful and homogeneous mixing of miscible hard substances and processes compacting powders designed to achieve various tablets (pills, compact sintering).

The current state of ultrasonic welding of dissimilar metallic materials. Analysis of current status on ultrasonic welding materials was based on documentary material selected from the webpage, development of research institutions renowned journals, specialized companies and world-renowned European and documentaries.

Internationally applied research in the delivery of specialized equipment and technologies unconventional combination of ultrasound in microelectronics, electronics, medical devices, consumer goods industry, etc., started several years.

Technical issues regarding the development of complex equipment for welding, integration in automated production lines that meet outstanding performance, have been and are being addressed in concrete.

Bibliographic research conducted orientation highlights research centers joining microtechnology, including ultrasonic joining Micro-technologies in the following strategic directions.

– Monitoring and modeling processes – has been developed and is widely applied in hardware configuration and software SPICE modeling thermal process application, vibration spectrum analysis, simulation diffusion processes, thermal fatigue analysis, elastic and plastic deformation, etc.

– Development of specialized modules for ultrasound in the design and analysis programs specific research activities – SPICE, I-DEAS, ABAQUS, ANSYS, etc.

– Development of ultrasonic welding of metallic materials: a) ultrasonic welding of similar materials aluminum, copper and steel with external energy intake; b) ultrasonic welding of dissimilar materials aluminum and silver silicone materials, ceramics and glass, materials engineering.

– Develop processes termosonic combination of wires:

- 1) termocompresion joints, ultrasonic and termosonic interconnections;
- 2) termosonic joining wire terminals Au, Al;
- 3) fixing ultrasound Au and Al terminals.

- Development of mechanical testing methods and tightness.
- Development corrosion test methods – attempt to moisture and elevated temperature, electrochemical dynamics analysis.

Internationally the specialized equipment manufacturers ultrasonic welding, elitist groups is relatively restricted among which remember: AMTECH Ultrasonic Welding, USA, BRANSON Ultrasonic Welding, USA, stapler Ultraschall Technik GmbH Germany SONOBOND Ultrasonics Industries Company USA; BRANSON Ultraschall EMERSON Technologies GmbH & Co. Germany, Italy ULTRASUONI Raimi.

Acknowledgements. This paper is supported by the Sectorial Operational Programme Human Resources Development (SOP HRD), financed from the European Social Fund and by the Romanian Government under the contract number POSDRU/159/1.5/133675.

REFERENCES

- Floricele D.I., *Joining Fiber Optics -I-Manufacturing Technology BRAMAT 2007*. Internat. Conf. on Mater. Sci. a. Engng., February 22-24, 2007, Braşov Romania. 3.32 Pag. 247
- Floricele D.I., Şerban C.E., Dozescu S., *Thermoplastic Piping Systems for Biotech Water Applications BRAMAT 2007*. Internat. Conf. on Mater. Sci. a. Engng., Braşov, February 22-24, 2007.
- Floricele D.I., Trif I.N., Şerban C.E., *Modern Technologies of Joining Plastic Material Pipes*. Internat. Conf. "Technology and Quality for Sustained Development", Bucureşti, May 25-27, 2006.
- Floricele D.I., Şerban C.E., *Innovative Cooling Design for Plastic Injection Molds*. Rev. de Materiale Plastice, 3 (2010).
- Karian H.G., *Handbook of Polypropylene and Polypropylene Composites*, ISBN: 0-8247-1949-21999.
- Kazmer D., *Injection Mold Design Engineering*. ISBN-10: 15699041702007
- Lewis R.W., *Fundamentals of the Finite Element Method for Heat and Fluid Flow*. ISBN 0-470-84788-32004.
- Lucian M., *Mecanica Fluidelor*. Curs Online Universitatea Politehnica Bucureşti, [Http://www.Hydrop.Pub.Ro/Mandreadoc.Htm](http://www.Hydrop.Pub.Ro/Mandreadoc.Htm)
- Lungu M., *Utilaje pentru prelucrarea polimerilor*. Univ. Tehnică „Gh. Asachi”, Iaşi, 1980.
- Malloy R., *Plastic Part Design for Injection Molding*. ISBN: 1-56990-129-51994.
- Munteanu A., Mladin I., *Promoting Inovation, Creativity and Technology Transfer Through a Web Platform for Research*. Proc. Internat. Conf. Quality Manag. A. Higher Education, QMHE 2010, 2010, 163-166.
- Soto-Acosta P., Colomo-Palacios R., Perez-Gonzalez D., *Examining Whether Highly E-Innovative Firms are More E-Effective*. Informatica, 35, 481-488 (2011).

* * Innovation Union Scoreboard 2011, <http://www.proinno-europe.eu> [5] OECD 2011. Science, Technology and Industry Scoreboard. Paris OECD.

INOVAREA ÎN SOCIETATEA BAZATĂ PE CUNOAȘTERE Tehnologia de sudare a plasticelor

(Rezumat)

Sunt prezentate informații de bază și câteva proprietăți importante în alegerea unui proces nou de către o companie aflată în strânsă legătură cu societatea bazată pe cunoaștere.

O societate a cunoașterii generează procese, acțiuni și pune la dispoziția tuturor membrilor societății cunoașterea, ce poate fi utilizată pentru îmbunătățirea condiției umane.

Sudarea cu ultrasunete este un proces legat de căldură, care poate crește în mod semnificativ producția și costurile de asamblare mai mici, folosit mai mult în designul auto al pieselor din plastic, oferind flexibilitate și versatilitate ce nu se regăsește în multe alte procese de asamblare.

Se prezintă efectul și metodele procesului de sudare în companiile de automobile ce se folosesc de inovare, într-o societate bazată pe cunoaștere. Sudare cu laser a materialelor plastice devine din ce în ce mai răspândită, deoarece oferă multe beneficii. Studiul prezintă metode de sudare pentru diverse produse realizate din materiale compozite raportat la un domeniu mare de parametri tehnologici și mecanici ai procesului de sudare.

COMBINED PROCESS FOR OBTAINING THE PARTS MULTILAYER

BY

ANIȘOARA CORĂBIERU^{1*}, PETRICĂ CORĂBIERU²
and DAN-DRAGOȘ VASILESCU²

¹“Gheorghe Asachi” Technical University of Iași
Faculty of Material Science and Engineering

²SC Procomimpex, Unit R&D and Engineering Technology of Iași

Received: March 3, 2014

Accepted for publication: March 25, 2014

Abstract: The joining temperature is the most important metallurgic factor that influences the characteristics and structure of the bimetallic layers obtained by immersion and vertical centrifugation. In order to outline the influence of the joining temperature, a series of parameters have been held constant, and assessments for different values of the joining temperature have been performed. Proper outcome was obtained at joining temperatures ranging between $T_{\text{join}} = 1,100^{\circ}\text{C}$ and $T_{\text{join}} = 1,160^{\circ}\text{C}$. Technological process is a combined process. Deposition of layers is carried out in the liquid phase. The completion of deposition is carried out in solid phase.

Keywords: combined method; bimetal; immersion–vertical centrifugation.

1. Introduction

The originality of this way of obtaining steel-bronze bimetal jacks by immersion and vertical centrifugation consists in its complete national novelty (Corăbieru *et al.*, 2007).

*Corresponding author: *e-mail*: acorabieru@yahoo.com

The procedure contributes to elimination of certain operations and equipment require for the pre-heating, handling of liquid metal, casting in classical centrifugal machines, and extraction. The process allows full automation, crossing and overlaying of the production processes, the deposition one and the bar and parts casting (Corăbieru & Corăbieru, 2004; Velicu *et al.*, 2008). The combined process is an embodiment of the multilayer pieces.

2. The Principle of the Experimental Procedure

The technological experimental principle for execution of steel-bronze bimetallic jacks consists of the immersion of the steel core in the bronze dip, lifting the core out of the dip until about half its length and its spinning with an appropriate angular speed required for the deposition to take place (Corăbieru & Corabieru, 2012b, 2013).

The centrifugal force that appears by spinning the core in the bronze dip determines the repartition of the bronze on the core steel walls, the adherence of the bronze layer and the diffusion of the atoms at the steel-bronze interface, thus creating an inter-phase zone. The principle schema of executing bimetallic jacks by vertical centrifugation is presented in Fig. 1. The steel jack is immersed in the bronze dip and its spinning begins (Corăbieru & Corabieru, 2012b; Corăbieru *et al.*, 2007b).

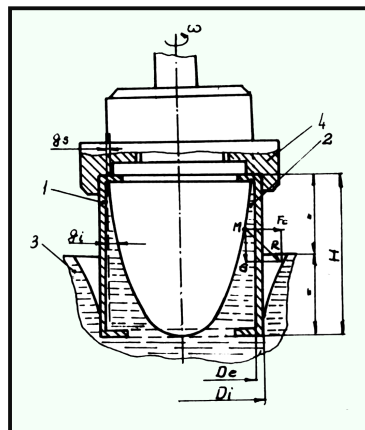


Fig. 1 – Principle scheme of the ICV process: 1 – steel core; 2 – the bronze layer distributed on the core walls; 3 – the bronze dip; 4 – fastening chuck.

3. The Experimental Installation

In the beginning time of the deposition process, the melted bronze does not have the angular speed uniform in all its layers, but gradually this speed gets uniformed and becomes equal to the angular speed of the steel core. It is under

these conditions that the spinning movement is stabilised and one can reckon that the spinning melted bronze finds itself in a relative rest situation, the space form of the free surface being a rotational paraboloid. After stabilising the spinning movement, the jack is gradually lifted up so that, when the optimal deposition speed is reached, the jack is immersed only a hint in the bronze dip (Corăbieru *et al.*, 2007a, 2007c).

The designed and built MC is the main device of the installation for execution of bimetallic jacks. The MC ensures the transport of the steel core to each and every working point of the equipment, executes the immersion of the jack core in the IDP, the CTI, and in IR, as well as the spinning movement of the jack in the bronze dip in view of executing the deposition by ICV. In Fig. 2, the MC and its designed principle scheme are presented.

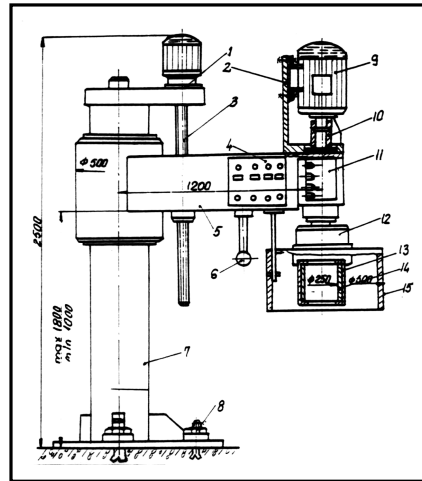


Fig. 2 – The centrifuge machine MC; *a* – the vertical centrifuge machine for execution of bimetals by ICV; *b* – the principle scheme of the designed and built MC; 1 – motor reduction gear for vertical movement; 2 – support for electric dc engine; 3 – screw-nut mechanism for vertical movement; 4 – control panel; 5 – folding arm; 6 – Handle; 7 – guiding axis; 8 – foundation bolts; 9 – dc engine; 10 – coupling; 11 – main shaft; 12 – mechanic lathe; 13 – Steel jack; 14 – deposited bronze layer; 15 – sliding cylindrical gasket.

4. Proposed Methods for Determining the Specific Adhesion

The specific adherence characterizes the bimetallic component parts for automobiles from a qualitative point of view.

For the calculation of the specific adherence the resistance of detachment by shearing is necessary to be determined (Corăbieru *et al.*, 2007d; Corăbieru *et al.*, 2008).

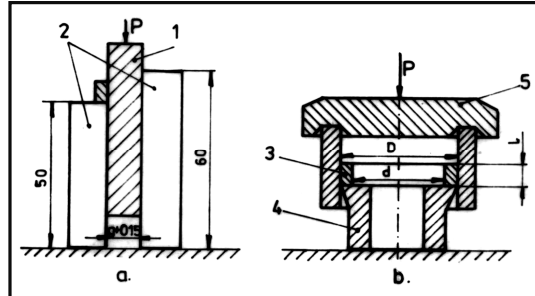


Fig. 3 – Proposed modalities of determination of the detachment resistance by shearing: *a* – determination of the detachment resistance with linear test bar; *l* – linear test bar; 2 – guiding stocks; *g* – structure of base support of OLT 35; *b* – determination of the detachment resistance with circular test bar; 3 – circular test bar type bushing-disc; 4 – matrix; 5 – superior support; *D* – inner diameter of base support of the bimetallic bushing; *d* – inner diameter of the bimetallic bushing.

In the Fig. 4, types of specimens used for the proposed modalities of determination of the detachment resistance by shearing are shown.

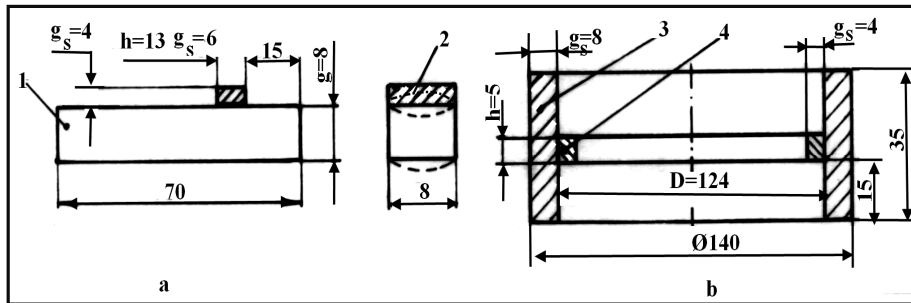


Fig. 4 – Types of specimens used for the proposed modalities of determination of the detachment resistance by shearing of the experimented bimetallic bushings: *a* – linear specimen; *l* – base material OLT35; 2 – bronze layer deposited by vertical spin casting, $g_s = 4$ mm; A – the area of the surface submitted to the detachment by shearing, $[mm^2]$, $A = h \times 8 = 1.5g_s \times 8 = 1.5 \times 4 \times 8 = 48$ mm^2 ; *b* – circular specimen type bushing-disc; 3 – support of base steel OLT 35, $\Phi 140 \times 8$; 4 – bronze layer deposited by vertical spin casting, $g_s = 4$ [mm]; *D* – inner diameter of the base support, [mm]; *h* – height of the deposited layer submitted to the detachment, [mm]; A – area of the surface submitted to the detachment by shearing, $[mm^2]$; $A = \pi Dh = \pi \times 124 \times 5 = 1946.8$ mm^2 .

The specific adherence (*q*) is determined with the formula:

$$q = F/A, [N/mm^2]$$

where: F – pressing or tensile force, [N]; A – area of the surface submitted to the detachment, [mm²].

Depending on the specific adherence value q , we can have:

- a) soft joint: $q < 70$ N/mm²;
- b) average joint: $q = 70 \dots 170$ N/mm²;
- c) strong joint: $q > 170$ N/mm².

5. Analysis of the Results

For the spotlight of the influence of the joining temperature into the framework of the experiments, the following parameters have been kept constant:

- a) dimensions of the base half-product $\Phi 140 \times 8$ OLT 35;
- b) deposited bronze layer: superior thickness $g_s = 4$ mm; inferior thickness $g_i = 12$ mm; final thickness after machining $g_0 = 4$ mm;
- c) length of steel support $L = 140$ mm;
- d) joining process duration = duration of maintaining at the regime rotation speed = 90 s;
- e) rotation speed: 500 rot/min.

Table 1

Influence of the Joining (Casting) Temperature on the Specific Adherence of the Experimental Bushings for Automobiles

Crt. Nr.	Joining Temp. T_{mb} , °C	Detachment resistance, specimens as per fig.4., $A =$ area of the surface detached by shearing = 48 mm ²		
		Applied force F , N	Specific adherence $q = F/A$ N/mm ²	Remarks
1	1020	2880	60	$Q < 70$ soft, non-conform
2	1040	3840	80	$q > 70$ average joint, low
3	1060	5760	120	$70 < q < 170$ average joint, middle
4	1080	7200	150	$70 < q < 170$ average joint, high
5	1100	9600	200	$q > 170$ strong joint
6	1120	9120	190	$q > 170$ strong joint
7	1140	8160	170	$q = 170$ strong joint
8	1160	7200	150	$70 < q < 170$ average joint, high

Metallographic structures of the samples have spotlighted the base material (MB), the deposited layer from the proximity of the joining zone (SD) as well as the interface steel –bronze, joining zone (ZI).

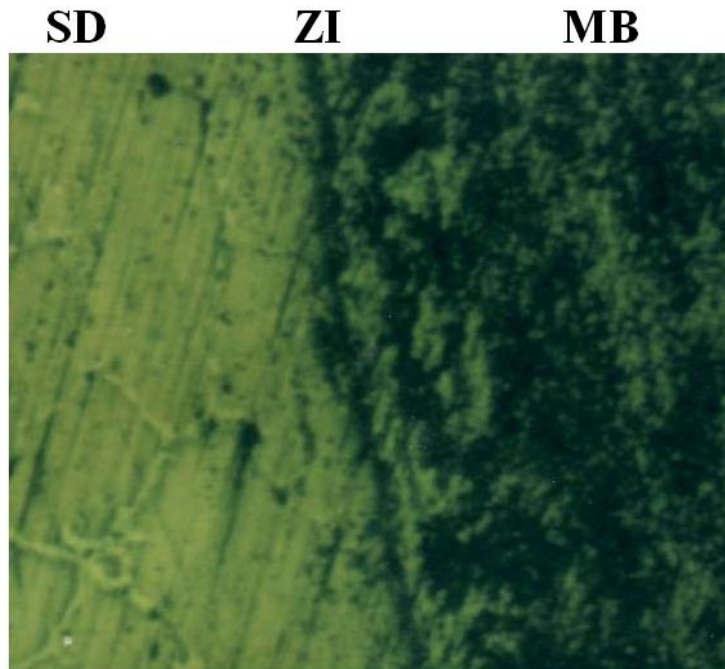


Fig. 5 – Bimetal structure OLT35-CuSn10 ($T_{\text{join}} = 1,120^{\circ}\text{C}$; $t_{\text{join}} = 140\text{ s}$; specific adhesion $q = 190\text{ N/mm}^2 \rightarrow$ hard joint). SD – s.s. α polyhedral + acicular inter – metallic compound Cu_3Sn , MB – ferrite + pearlite structure homogeneous, ZI – crossing area, dissolved oxides and small, chemical bonds by diffusion elements.

The non-conform joints have presented the following structure: SD – s.s. α + acicular inter-metallic compound Cu_3Sn ; MB – gross ferrite + perlite; ZI – portions where the partial fusion and the apparition of the joining knots take place;- the oxides are maintained in singular places between layers.

The joints with a high specific adherence have presented a structure like this: SD – s.s. α polyhedral; MB – ferrite-perlite structure; ZI – passing zone; oxides are dissolved, chemical compounds.

6. Aspects of the Final Heat Treatment

The heat treatment of homogenization annealing has in view the following aspects:

1° Elimination of the dendrite segregation (the chemical composition defects from the inside of the deposited layer SD crystals, that alters the properties creating phases out of equilibrium).

2° Re-heating at as higher temperature, maintaining a sufficient period of time for the proper distribution by diffusion of the components.

3° The technological parameters of the annealing homogenization have been experimentally determined:

Bimetal OLT35-CuSn10: $T_{\text{ann}} = 650-700^{\circ}\text{C}$, $t_{\text{maintain}} = 5-8\text{min/mm thick}$. wall $\sim 0,5\text{h}$, cooling in quiet air.

Bimetal OLT35-CuSn4Zn4Pb17: $T_{\text{ann}} = 650^{\circ}\text{C}$, $t_{\text{maintain}} = 0,5\text{ h}$, cooling in quiet air.

4° Important modifications of the SD structure are produced (structure with dendrite segregations \rightarrow homogeneous mono-phase or bi-phase structure).

5° For MB this treatment is equivalent with a complete stress relieving annealing, the level of the remnant stresses decreasing at values under 5 daN/mm^2 concomitantly with hydrogen elimination.

In Fig.6 the diagrams of the heat treatments experimented for the bimetallic hypoeutectoid carbon steel – bronze are shown.

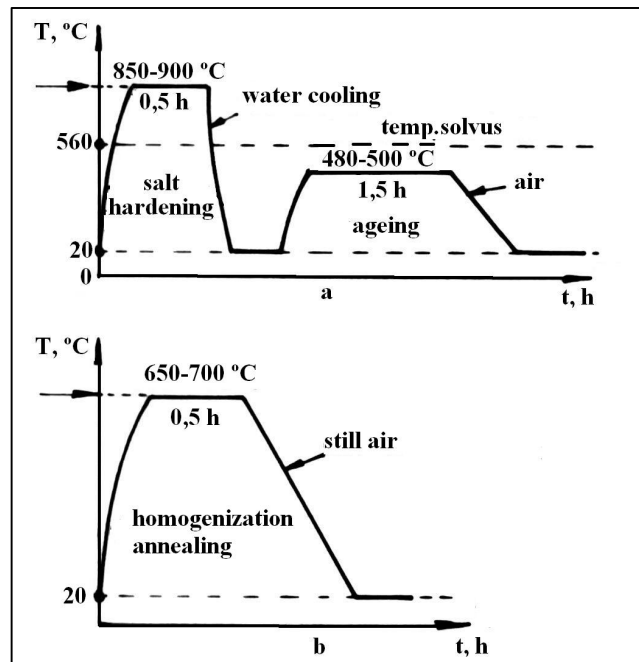


Fig. 6 – The heat treatment of the experimented bimetallic bushings for automobiles, made of hypoeutectoid carbon steel – bronze: *a* – OLT35-CuAl9T \rightarrow salt hardening + ageing; *b* – OLT35- CuSn10, OLT 35- CuSn4Zn4Pb17 \rightarrow homogenization annealing.

7. Economic Aspects on the Experimental Procedure

By the utilization of the half-products and bushings with bimetallic layers the following aspects are had in view :

i) saving of the expensive and critical materials and implicitly the imports reducing;

iii) obtaining a product that combine various properties, unreachable by using of a single metal:

a) the good thermal conductivity of the base steel with the corrosion-proof of the deposited steel;

b) high strength of the base steel with anti-friction good properties of the deposited alloy;

c) high mechanical properties and thermal dilatation coefficients different between component metals of the thermo-bimetal;

d) high technological properties of the base steel with distinct appearance of the deposited materials.

The thickness of the half-products and bimetallic bushings most utilized in the whole world is comprised between 0.5...5 mm, the proportion of the deposited layer SD being of 10%,...,30%.

In Fig. 7 the variation of the ratio between the production cost of the monoblock massive half-product and the cost of the carbon steel – stainless high alloyed steel bimetallic half-product is presented, conforming to the economic studies effected in Germany and France.

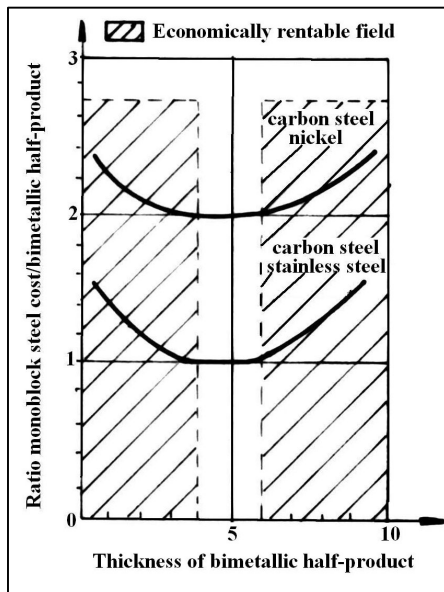


Fig.7 – Variation of the ratio between the production cost of the half-products of monobloc metallic materials and the cost of the bimetallic half-products with deposited layer SD of these materials.

Conforming to Fig. 7 it is marked that for the thicknesses of the bimetal under 3...4 mm the economic advantage is increasing (the bimetal production is rentable), as well as for thicknesses over 5 mm.

Using the half-products and the bimetallic bushings low alloyed carbon steel – bronze, the percentage savings presented in Table 2 are obtained.

Table 2
Average Savings Achieved by the Obtaining and Utilization of the Bimetals Low Alloyed Carbon Steel -Bronze

Cr. nr.	Savings resulted by the utilization of the bimetals low alloyed carbon steel - bronze	Proportion of deposited layer SD, %	
		10%	20%
1	Value savings	39	24
2	Quantitative savings regarding the alloy of deposited layer SD	81	65
3	Minimum ratio between the price of the deposited alloy SD and the price of the base material MB in order to achieve value savings	4	5

Indicative calculations in order to establish the costs of some half-products and bimetallic bushings carbon steel–copper and carbon steel-bronze with the proportion SD 15%, by comparing with the technological proceedings are presented in the Table 3.

Table 3
Comparative Costs of the Half-Products and Bimetallic Bushings Depending on the Technological Proceedings

Cr. nr.	Manufacture proceeding	Estimative cost		
		France, Germany, Sweden	Russia, Ukraine	Romania
1	Method of compound ingot, [%]	118	120	120
2	Method of compound package, [%]	123	127	125
3	Method of welding in slag bath, [%]	105	105	105
4	Centrifugal methods, [%]	100	100	100

From the Table 3 it is remarked that the most advantageous proceedings from the economic point of view are those based on centrifugal methods → much more the real possibilities of the immersion and centrifugation proceedings which eliminate operations and equipment necessary to pre-heating, manipulating, casting into spin casting machines, extraction.

Having in view a possible series production in Romania, the products would be competitive on the European market taking into account that for a period of time the expenses with the man power will be low.

8. Conclusions

At joining temperatures $T_{\text{join}} = T_{\text{top1}} + 100$, the specific adherence reaches values $q > 170 \text{ N/mm}^2$ corresponding to the strong joints.

At joining temperatures $T_{\text{join}} > T_{\text{top1}} + 100$, the specific adherence decreases towards values of 150 N/mm^2 corresponding to the average joints.

Joining temperature does not significantly influence the thickness of the deposited layer.

At very high joining temperatures over the optimum determined limit, the joint is no more strong, the resistance of the joint decreases due to the acceleration of the carbon diffusion into the bronze, to the increase of depth of carbon penetration into the bronze, to the high decarburation of the base steel and of the high carburization of the bronze surface, in this way appearing the inter-crystalline corrosion.

Homogenization annealing of the bimetallic components for automobiles has in view the elimination of the dendrite segregation that creates phases out of equilibrium leading to the reducing of the specific adherence between layers and to exfoliation.

The gradual increasing of the geometrical dimensions bushings leads to the increasing of the economical advantages in the case of the utilization for welded constructions of big dimensions.

Acknowledgement. This work was supported by a grant of the Romanian National Authority for Scientific Research CNDI – UEFISCDI, project number 185/2012.

REFERENCES

- Corăbieru A., Corăbieru P., Sohaciu M., Vasilescu D.D., *Industrial Applications of the Bimetallic Bushings Economic Aspects*. Bul. Inst. Politehnic, Iași, **LIII (LVII)**, 2, s. Mater. Sci. a. Engng., 225 (2007d).
- Corăbieru A., Corăbieru P., *Bimetallic Cylinders Made by Assembling Axle-Barrel from the Casting*. 2004, ISBN 973-702-020-0.
- Corăbieru A., Corăbieru P., *Elements of Industrial Competitive Analysis*. Bul. Inst. Politehnic, Iași, **LVIII (LXII)**, 4, s. Mater. Sci. a. Engng., 7-15 (2012b).
- Corăbieru A., Corăbieru P., Predescu C., Vasilescu D.D., *Study of the Processing by Heat Treatments of Bimetallic Bushings for Automobiles, of Hypoeutectoid Carbon Steel – Bronze*. Bul. Inst. Politehnic, Iași, **LIII (LVII)**, 2, s. Mater. Sci. a. Engng., 221 (2007b).
- Corăbieru A., Corăbieru P., *Technological Process for Obtaining the Superficial Layers by Combined Processing*. Bul. Inst. Politehnic, Iași, **LVIII (LXII)**, 3, s. Mater. Sci. a. Engng., 13-19 (2012a).

- Corăbieru A., Corăbieru P., *Tendencies and Influences of the Sustainable Development Regarding the Occupational Safety and Health*. Bul. Inst. Politehnic, Iași, **LIX (LXIII)**, 3, s. Mater. Sci. a. Engng., 9-19 (2013).
- Corăbieru A., Corăbieru P., Velicu S., *Study of the Influence of the Heat Treatments on the Hardness of the Ecological Quaternary Alloys*. Proc. of the 16 th Internat. Conf. on Manufact. Syst. (ICMaS), Ed. Acad. Române, București, 2007a, 41-44, 22-11.
- Corăbieru A., Corăbieru P., Vasilescu D.D., *Economic Aspects of the Bimetallic Bushings*. Tehnologia Inovativă, Revista Construcția de Mașini, **59**, 1, 61 (2007c).
- Corăbieru C., Vasilescu D.D., Corăbieru A., Corabieru P., *Steel – Bronze Bimetal by Immersion and Vertical Centrifugation*, Bul. Inst. Politehnic, Iași, **LVIII (LXII)**, 4, s. Mater. Sci. a. Engng., 7-15 (2012).
- Corăbieru P., Corăbieru A., Vasilescu D.D., *Heat Treatments of Bimetallic Bushings*. Bul. Inst. Politehnic, Iași, **LIV (LVIII)**, 1, s. Mater. Sci. a. Engng., 235-240 (2008).
- Velicu S., Zaiț D., Corăbieru P., Corăbieru A., Vasilescu D.D., *Aspects Regarding the Improvement of the Life Metallic Products Management in the Industry of Auto Components*. Metalurgia Internat., Edit. Științifică FMR, **XIII**, 9 (2008).

PROCEDEU COMBINAT DE OBȚINERE A PIESELOR MULTISTRAT

(Rezumat)

Temperatura de îmbinare este cel mai important factor metalurgic care influențează caracteristicile și structura straturilor bimetalice obținute prin imersie și centrifugare verticală. În scopul de a sublinia influența temperaturii de îmbinare, o serie de parametri au fost menținuți constant și au fost efectuate determinări pentru diferite valori ale temperaturii de îmbinare. Rezultate corespunzătoare au fost obținute la temperaturi cuprinse între $T_{imb.} = 1100^{\circ}\text{C}$ și $T_{imb.} = 1160^{\circ}\text{C}$. Procedul tehnologic este un procedeu combinat. Depunerea se realizează în fază lichidă și se consolidează în fază solidă.

